AFRL-VA-WP-TR-1999-3039

BACTERIORHODOPSIN SOL-GEL FOR HOLOGRAPHIC APPLICATIONS

JAMES MILLERD, PH.D.

METROLASER, INC.
18010 SKYPARK CIRCLE #100
IRVINE, CA 92614-6428

APRIL 1999

FINAL REPORT FOR 09/19/1996 – 02/19/1999

THIS IS A SMALL BUSINESS TECHNOLOGY TRANSFER RESEARCH (STTR) PHASE II REPORT

APPROVED FOR PUBLIC RELEASE; DISTRIBUTION UNLIMITED

AIR VEHICLES DIRECTORATE
AIR FORCE RESEARCH LABORATORY
AIR FORCE MATERIEL COMMAND
WRIGHT-PATTERSON AIR FORCE BASE OH 45433-7542

NOTICE

USING GOVERNMENT DRAWINGS, SPECIFICATIONS, OR OTHER DATA INCLUDED IN THIS DOCUMENT FOR ANY PURPOSE OTHER THAN GOVERNMENT PROCUREMENT DOES NOT IN ANY WAY OBLIGATE THE US GOVERNMENT. THE FACT THAT THE GOVERNMENT FORMULATED OR SUPPLIED THE DRAWINGS, SPECIFICATIONS, OR OTHER DATA DOES NOT LICENSE THE HOLDER OR ANY OTHER PERSON OR CORPORATION; OR CONVEY ANY RIGHTS OR PERMISSION TO MANUFACTURE, USE, OR SELL ANY PATENTED INVENTION THAT MAY RELATE TO THEM.

THIS REPORT IS RELEASABLE TO THE NATIONAL TECHNICAL INFORMATION SERVICE (NTIS). AT NTIS, IT WILL BE AVAILABLE TO THE GENERAL PUBLIC, INCLUDING FOREIGN NATIONS.

THIS TECHNICAL REPORT HAS BEEN REVIEWED AND IS APPROVED FOR PUBLICATION.

Glenn W. Williams

Glenn W. Williams
Electonic Engineer
Aerodynamic Configuration Branch

Donald J. Stava

Don Stava
Aerodynamic Configuration Branch
Aeronautical Sciences Division

John A. Bowlus

for James Rudd
Aeronautical Sciences Division
Air Vehicles

Do not return copies of this report unless contractual obligations or notice on a specific document requires its return.

REPORT DOCUMENTATION PAGE

Form Approved OMB No. 0704-0188

1. AGENCY USE ONLY *(Leave blank)*	2. REPORT DATE	3. REPORT TYPE AND DATES COVERED
	APRIL 1999	FINAL REPORT 09/19/1996 - 02/19/1999

4. TITLE AND SUBTITLE

BACTERIORHODOPSIN SOL-GEL FOR HOLOGRAPHIC APPLICATIONS

5. FUNDING NUMBERS

C: F33615-96-C-3016
PE 65502
PR STTR
TA FI
WU 02

6. AUTHOR(S)

JAMES MILLERD, PH.D.

7. PERFORMING ORGANIZATION NAME(S) AND ADDRESS(ES)

METROLASER, INC.
18010 SKYPARK CIRCLE #100
IRVINE, CA 92614-6428

8. PERFORMING ORGANIZATION REPORT NO.

TWP8JMF.DOC

9. SPONSORING/MONITORING AGENCY NAME(S) AND ADDRESS(ES)

AIR VEHICLES DIRECTORATE
AIR FORCE RESEARCH LABORATORY
AIR FORCE MATERIEL COMMAND
WRIGHT-PATTERSON AFB, OH 45433-7542
POC: GLENN WILLIAMS, AFRL/VAAA, 937-255-2493

10. SPONSORING/MONITORING AGENCY REPORT NUMBER

AFRL-VA-WP-TR-1999-3039

11. SUPPLEMENTARY NOTES

THIS IS A SMALL BUSINESS TECHNOLOGY TRANSFER RESEARCH (STTR) PHASE II REPORT

12a. DISTRIBUTION/AVAILABILITY STATEMENT

APPROVED FOR PUBLIC RELEASE, DISTRIBUTION UNLIMITED

12b. DISTRIBUTION CODE

16. ABSTRACT *(Maximum 200 words)*

Many Bacteriorhodopsin (BR) mutants were synthesized and their optical absorption properties were measured. Several of the mutants were identified that formed the so-called "Q390 state" at neutral pH, but the ultra-long storage lifetime of this state was not investigated. The double mutant D85N/V49A showed a factor of 50 increase in holographic recording sensitivity compared with the single mutant D85N, and had similar diffraction efficiency. The increased sensitivity of this mutant in the spectral range of laser diodes and its long storage lifetime makes this film a good choice for real-time holographic interferometry systems and optical data storage applications.

It was demonstrated that a compact diode laser could be used to record and reconstruct holograms in thick films of the mutant D85N. It was demonstrated that lifetimes of several weeks could be achieved. Since diffusion limits the lifetime, using cross-linked BR can substantially increase it. It was also demonstrated that very high data densities could be achieved using shift multiplexing with a speckle wave reference beam. With improved materials (reduced scattering, crosslinked polymer host), a 3 mm thick CD-ROM sized disk of D85N could potentially be used to store hundreds of Gbytes of information.

14. SUBJECT TERMS

STTR Report, bacteriorhodopsin, photochromic material, holographic storage material, optical data storage

15. NUMBER OF PAGES

43

16. PRICE CODE

17. SECURITY CLASSIFICATION OF REPORT	18. SECURITY CLASSIFICATION OF THIS PAGE	19. SECURITY CLASSIFICATION OF ABSTRACT	20. LIMITATION OF ABSTRACT
UNCLASSIFIED	UNCLASSIFIED	UNCLASSIFIED	SAR

NSN 7540-01-280-5500

Standard Form 298 (Rev. 2-89)
Prescribed by ANSI Std. 239-18
298-102

TABLE OF CONTENTS

TABLE OF FIGURES

LIST OF TABLES

1. PROJECT SUMMARY

1.1 Project Objectives

The goal of this project was to develop an erasable optical storage medium that is useful for high speed interferometry and holographic data storage. To accomplish this goal, we developed novel varieties of the photochromic material, bacteriorhodopsin (BR), and encapsulating it in thick volume elements. Bacteriorhodopsin is an organic, photochromic material that has demonstrated exceptional promise as a real-time holographic material.[1,2] Through genetic engineering, the optical properties of BR, including spectral response and storage lifetime, can be significantly modified for optimal performance in specific applications.[3]

During the Phase I research we investigated fabricating novel optical materials in various shapes and configurations using sol-gel, epoxies and polymeric hosts. Incorporation of BR into a large, centimeter thick, volume element permits the usage of multiplexed holographic storage. Volume holographic media have numerous potential applications of interest to both the Air Force and the commercial sector including high-speed holographic cameras,[4] 3-D optical data storage,[5] and optical signal processing.[2]

This collaborative STTR program teamed university researchers at Wayne State University and the University of California, Irvine, who are experts in the engineering, production and characterization of BR, with two small businesses: Bend Research and MetroLaser, who are experts in polymer encapsulation and in applications of non-linear optical materials, respectively. The team members for this research effort were selected for their individual strengths in these related fields.

Specific objectives of this program were:

1. Optimize the holographic characteristics of BR using mutagenesis.
2. Develop an economical method to produce BR volume elements.
3. Develop and demonstrate a prototype holographic interferometer system.
4. Demonstrate a Read/Write/Erase digital optical memory breadboard.

1.2 Project Accomplishments

During the course of this Phase II SBIR program we were able to:

- Synthesize over 50 new mutants.
- Identify a new mutant that had a factor of 50 improvement in sensitivity.
- Develop a fabrication procedure for producing thick volume elements.
- Develop a compact holographic data storage breadboard.
- Identify and characterize a new holographic multiplexing technology.
- Develop a real-time holographic breadboard system and demonstrate fast, quantitative data reduction.

These accomplishments have resulted in the submission of three publications to prestigious technical journals. Further, they constitute a proof of concept demonstration for our commercialization effort. In particular, we are targeting the real-time interferometer system for our initial commercial product. Although a holographic data storage system remains a long term goal, an immediate opportunity exists for the interferometer system. In the following document we describe in greater detail the scope and significance of our accomplishments.

2. BACKGROUND

2.1 Description of Bacteriorhodopsin

The uniqueness of BR lies in its biological origin. Bacteriorhodopsin is a protein found in the cell membrane of *Halobacterium Halobium*, a bacterium found naturally in salt flats. This molecule is located in sheets called "purple membrane" of approximately 1 μm that have a two-dimensional, hexagonal crystal structure. The molecule exhibits exceptional stability toward denaturation due to the crystalline nature of the purple membrane (Stoeckenius and Bogomolni, 1982; Henderson et. al., 1990) and a richness of photochromic activity not found in the non-biological world. These purple-membrane sheets are the building blocks of the BR-based volume holographic recording materials that were demonstrated during Phase I.

2.1.1 The Photocycle of BR and the Recording of Images

As illustrated in Figure 1a, BR acts as a light-driven proton pump, which is used by the bacterium for energy production under anaerobic conditions. The light-absorbing group of BR is retinal. Absorption of a photon by the retinal induces several successive photochromic shifts, each to a metastable state with different absorbance spectra. The mechanisms responsible for these photochromic effects are different from the mechanisms by which photochromic effects take place in conventional non-biological, dye-based materials used for optical-processing applications. A BR system would be difficult, if not impossible, to make synthetically; however, BR can be genetically engineered to possess the desired optical properties. Alterations in the amino acid sequence of the protein (by site-specific mutagenesis) can change the photochromic effects. Thus, tailoring of the photochromic response to specific applications is possible. This is one of the unique features of bacteriorhodopsin compared with conventional materials.

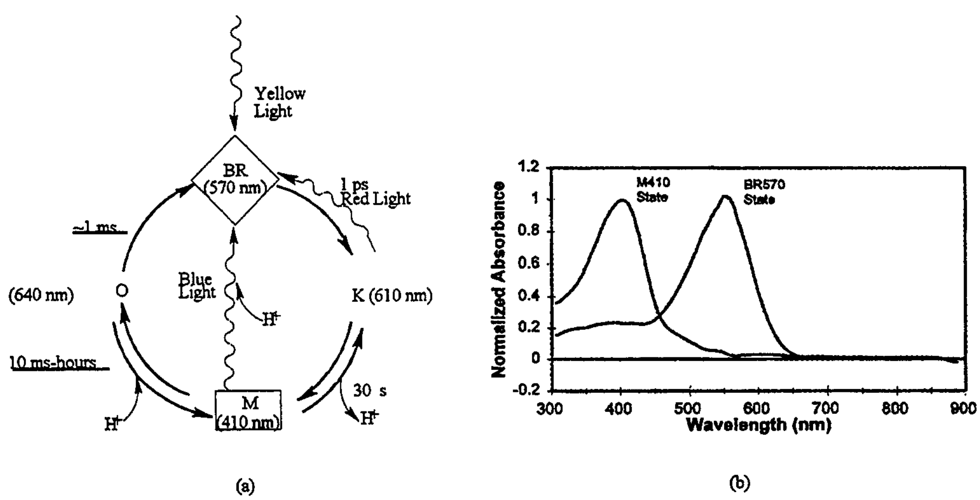

Figure 1. (a) Simplified Photocycle of Native BR and (b) Absorbance Spectrum in a Polymer Film.

When BR is illuminated with visible light, a number of events occur, as illustrated in Figure 1. First, photo-isomerization of the retinal occurs, and the absorbance peak of BR (initially at about 570 nm before illumination, i.e., the BR570 state), shifts in less than a picosecond to 610 nm. This initial process is very efficient, having a quantum efficiency of nearly 70%. Second, a series of changes in the absorbance spectrum occur due to thermally activated transitions to other intermediate states. Each change in the absorbance spectrum defines a different intermediate state. A key to the photocycle is the deprotonation step, which causes a substantial shift of the absorbance peak to 410 nm (the M410 state). This is normally the longest-lived state in the photocycle of BR. Third, the BR molecule returns to its initial BR570 state through other short-lived intermediates. The complete cycle of changes in absorbance following illumination by visible light comprises the BR photocycle (Figure 1a).

The lifetime of the M410 state for native BR ranges from a few milliseconds to hours (at room temperature), depending upon the chemical and physical environment of the BR. In holographic recording films made with BR, the time the image remains can be tuned by varying the environment (such as pH) into which BR is placed, which controls the M410 lifetime. Light near 410 nm also initiates a transition back to the BR570 state. Thus, the images recorded onto BR films can be photo-erased with blue light after being written on with yellow, green, or red light.

Patterns, such as holograms, are first written by photo-bleaching the BR570 state with light at a wavelength between 530 and 640 nm. The patterns can be subsequently read as positives (with light falling in the spectral absorption region of BR570) or as negatives (by reading with blue light in the spectral absorption region of the M410 state). In both cases, reading of the image can degrade the image itself due to photo-conversion of the exposed areas and bleaching of the unexposed areas.

2.1.2 Blue Membrane BR

2.1.2.1 THE Q390 STATE

A highly attractive method for recording data is using the so-called Q390 state. The Q390 state has no direct thermal pathway to relax to the ground state and therefore it is very long lived. In addition, in certain materials it is believed that it can be accessed using a multi-photon process which leads to the possibility of non-destructive readout.[6] There are two potential methods for accessing the Q390 state: optically through the O-state and thermally with blue membrane materials.

The photocycle for entering the Q390 state optically through the O-state is shown in Figure 2. The BR molecule ground state is shown as ***B***. Upon exposure to green/yellow light (570 nm), the molecule cycles through the ***M***, ***N*** and ***O*** states. The ***N*** state has a pathway to the ground state that requires absorption of 560 nm light. Because the cycle lifetime from the ***B*** to the ***N*** state is 50 - 100 micro seconds, illumination from a short pulse (less than 50 μs) can initiate the photocycle without driving the ***N*** to ***B*** reaction. Once in the ***O***-state, the molecule can thermally decay back to ***B*** or undergo a branching reaction in response to ~640 nm excitation. The branching reaction leads to a ***P*** state and subsequently a ***Q*** state. The ***P*** and ***Q*** states are quite interesting in that they have very long thermal lifetimes and can be driven back to the ground state (***B***) by excitation with

490 and 380 nm light, respectively. One possible scheme for long term data storage is to initially excite the BR medium with a spatially uniform, short pulse of 570 nm light. This light does not need to be coherent and could be generated by a filtered flash lamp or green LED. A short time later, after the molecules have cycled to the ***O*** state, the hologram is exposed at 670 nm. This drives the branching reaction and records the hologram in the ***P*** and or ***Q*** states. The stored holographic image can now be reconstructed by illumination with the original 670 nm reference beam. Because the 670 nm beam does not excite the ***B*** to ***M*** transition, the hologram is read non-destructively at the original recording wavelength. Reconstruction with the original recording wavelength is important to avoid aberrations in the reconstructed image and obtain maximum data storage density. The entire memory can then be erased by exposure to short wavelength (490-380 nm) light. The erasure light does not need to be coherent and could once again be generated by a flashlamp or blue LED.

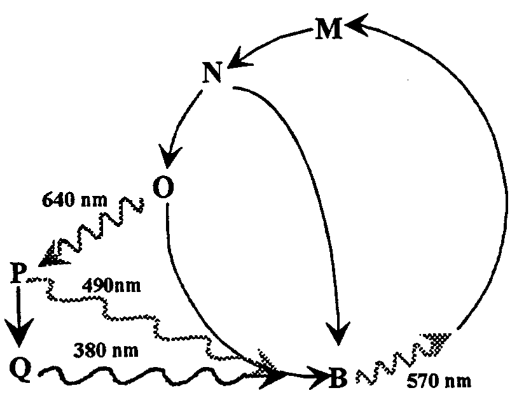

Figure 2. Modified photocycle for *O*-state bacteriorhodopsin. P and Q states can have very long thermal lifetimes and which can be read non-destructively with red ~670 nm light.

3. NEW MUTANT PRODUCTION AND CHARACTERIZATION

3.1 Summary

The primary research directions in the production of new mutants was:

A) Identify ***blue membrane analogs*** with improved sensitivity (relative to the material studied in Phase I - D85N/D96N)
B) Identify mutants that can efficiently form the Q390 state for use as an ultra-long storage lifetime material. This direction explored both ***long O-state mutants***, which were believed to form Q390 through an optical mechanism, and ***blue membrane analogs*** that can form this state through a thermal process.

We synthesized and measured the optical absorption properties of over 50 mutants. We were successful at producing long O-State materials, extending lifetimes by two orders of magnitude (10 ms to 1 sec); however, the long O-state materials had poor sensitivity converting to the P490 state and did not convert to the Q390 state using optical or thermal pathways. Therefore, the research into long O-state materials did not produce fruitful results. Research into blue membrane analogs was more productive. Several mutants were identified that form the so-called "Q390 state" at neutral pH; however, they were identified late in the research and were not fully characterized. The double mutant D85N/V49A had significantly improved optical properties over D85N/D96N. We produce significant quantities of this material and fabricated several thin films. D85N/V49A showed a factor of 50 increase in holographic recording sensitivity compared with the single mutant D85N. The film had a measured storage lifetime of over 27 days, ten times longer than previous films. The increased sensitivity of this mutant and its long storage lifetime makes this film a good choice for real-time holographic interferometry systems and optical data storage applications. In the following we discuss the research findings in greater detail.

3.1.1 Blue membrane analogs

During Phase I the mutant D96N/D85N was investigated as a possible long-storage lifetime material. Films prepared with this mutant had a blue color at neutral pH. The results obtained with the D96N/ D85N BR sample were very encouraging. Holograms were recorded in the material that lasted in excess of three days. Unfortunately, the film had a sensitivity that was roughly 1 to 2 orders of magnitude less than D96N/46V films. One of the primary goals of this work was to improve the sensitivity of these blue films.

The single mutation D85N causes BR to change from red to blue in color at neutral pH while the D96N mutation alone extends the M-state lifetime.[7] Since the M-state plays little if any role in the photocycle of D96N/D85N, it was speculated that the D85N is the important mutation in this material. Therefore, we examined all of the possible mutations at site 85 (single mutation) to see how the optical properties are altered. In addition, random mutations were performed, starting with D85N, to produce double and triple mutants.

3.1.2 O-state materials

The possibility of recording holograms via the ***O***-state is a technique that has only recently been explored and looks very promising.[8] For this reason, ***O***-state materials were investigated during the Phase I and II studies. To achieve maximum sensitivity it is desirable to have a material with a short ***M*** state and a long ***O***-state.

Wayne State University performed site-specific mutagenesis during this study to alter the BR and create long life ***O***-states. Our physical understanding of the O state is perhaps the weakest of all the states of the photocycle. ***O*** is formed in the last step of the photocycle and is a red-shifted state. The recovery of the bacteriorhodopsin ground state from ***O*** requires the loss of a proton from the acceptor of the Schiff base proton, D85 and the gain of this proton by a residue, ***X***, which serves as the release group for the proton on the extracellular side in the next photocycle. Following a clue provided by the work of Ebrey and Balashov, we showed that ***X*** was E204. It was then logical to assume that if E204 was mutated to an amino acid that could not accept a proton, say E204Q, then the lifetime of ***O*** would be increased. This was indeed the case, and we published a paper detailing these results (*Biochem*. No. 35 pp. 4054-62, 1996). In a more recent submission we have been able to show that the deprotonation of D85 during O decay occurred coincidentally with the reprotonation of the deprotonated E204 (really an E204D mutant which was used for technical reasons). Despite a considerable distance between D85 and E204, they interacted, possibly through a hydrogen bonded network that extends between them.

3.2 Mutant Production

To meet the need for holographic recording films that have superior properties, we constructed mutants in the gene coding for Bacteriorhodopsin (*bop*) using an expression system that we have recently developed. In this system, mutant Bacteriorhodopsins are synthesized in their natural host and not in *E-coli*, as in the classical method. This method allows the rapid and facile production of large quantities of mutant proteins.

In this and other investigations, the procedure is to construct mutants which are likely to have some effect on one property (either photocycle or photonic), and to test the hypotheses that arise from these observations by the construction of additional single or multiple mutants.

3.3 Mutant Screening Procedures

During the course of the Phase II research it was necessary to rapidly screen new mutants to see if the optical characteristics of the BR were favorably altered. Because the BR can have significantly different properties when encapsulated in a polymeric host than in an aqueous suspension, it is important to characterize the BR in a representative host. Production of a holographic quality film requires large quantities of BR and is time consuming, therefore, it is important to develop a method for rapidly evaluating small quantities of BR in a model host.

We determined that a polyacrylamide gel can be used to produce optical characteristics similar to that of gelatin films. Although the optical quality of the gels is not high it is sufficient for

absorption studies. The gels can be quickly made in plastic or quartz cuvettes to permit optical interrogation.

A simple screening procedure was developed for the "blue-film" materials that permitted screening for lifetime or sensitivity. Figure 3 shows the experimental setup where a lamp is used to probe the sample at a fixed wavelength. The wavelength is selected by placing a filter in front of the lamp. A photomultiplier tube monitors the light transmitted through the sample. A laser is used to pump the sample. Depending on the sample and the transition of interest the pump laser may be a doubled YAG (532 nm) HeNe (633 nm) or laser diode (690 nm). Light transmitted or scattered from the pump laser is used to trigger the analog-to-digital board which then records the sample transmission as a function of time. To screen for lifetime (e.g., o-state materials), a repetitively pulsed laser was used. Many cycles were averaged and the exponential lifetime was calculated. To screen for sensitivity (e.g., D85N analogs) a CW laser is used to pump the sample and the change in transmission for a given energy input is calculated. From this, the sensitivity of the material can be compared with existing baselines for the known mutants.

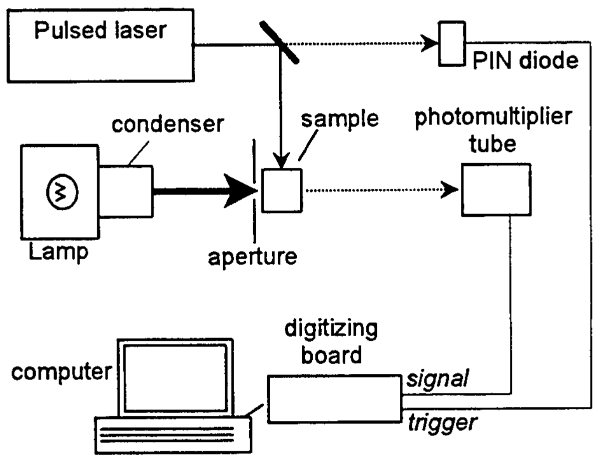

Figure 3. Experimental setup for fast screening mutants in gels.

3.4 Absorption Study Results

3.4.1 D85N Results

Wayne State produced large quantities of the mutant D85N (over 1000 mg of purified membrane). The mutant was characterized by optical absorption at Wayne State and at Bend Research after encapsulating the BR into a film.

Figure 4 is a graph of the spectra for the initial, photobleached, and erase states. The recording laser was a krypton-ion operating at 676 nm with a fluence of 0.9 J/cm^2. The total storage time was 17 hours before erasure. The erasure light was a filtered tungsten halogen light (center wavelength at 440 nm, width of 50 nm) with an approximate fluence of 10 mJ/cm^2 (the total erase time was 1 minute). The mutant formed the P490-state as expected; however, its spectrum is somewhat different than the 85/96 mutant used in Phase I. Most notably the mutant shows a more complete bleaching which should result in higher refractive index changes and higher

diffraction efficiency. This effect is evident by comparing the shape of the bleached or 490 state in Figures 1 and 2.

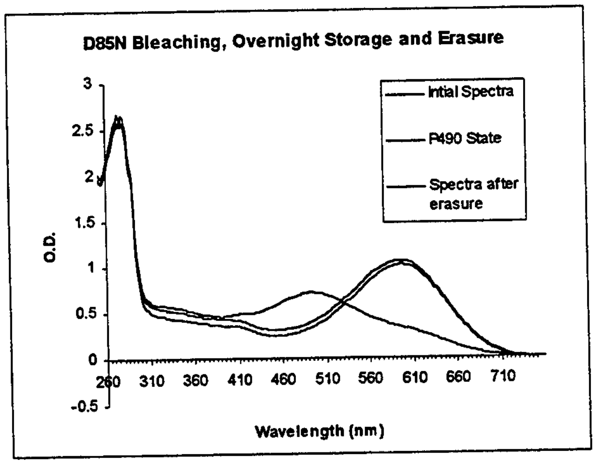

Figure 4. D85N Absorption spectra with and without pumping.

At room temperature D85N does not appear to form Q states. We recently verified that at elevated temperature the P490 state does indeed form Q380. Figure 5 shows the change in the difference spectrum (referenced to the initial B605 state) that occurs when the film is subsequently heated. The P490 state decreases markedly, the B605 shows a small increase and the Q380 state begins to appear. Figure 6 clearly illustrates the change in states by referencing the same spectra with respect to the initial P490 bleached state. Here the increase at 490nm is clearly seen. The eraseability of the Q490 state was measured in a preliminary set of experiments shown in Figure 7. The film was cooled to near room temperature and exposed to 457 nm light. This caused strong erasure of P490 states back to B605 and very weak depletion of Q380 states. By warming to 45C and illuminating with 457 nm light the Q380 state was depleted; however, a strong absorption feature appeared at 340 nm that is an indicator of free retinal which occurs due to catastrophic damage to the BR. Therefore, the heated erasure does not appear to be a viable alternative. It is possible that erasure with a shorter wavelength near 380 nm at room temperature could be more effective; however, this was not investigated further.

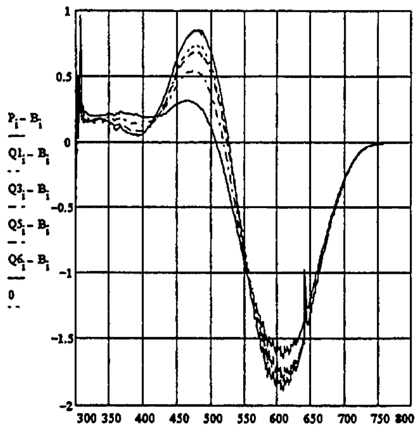

Figure 5. P = bleach film with 670nm, 25 J/cm^2 light at ~ 35°C for 40 min; Q1 =film heated at 50^{0}C for 10 min; Q3 =film heated at 50^{0}C for 25 min; Q5 =film heated at 50^{0}C for 100 min; Q6 =film heated at 50^{0}C for 11 hr 16 min.

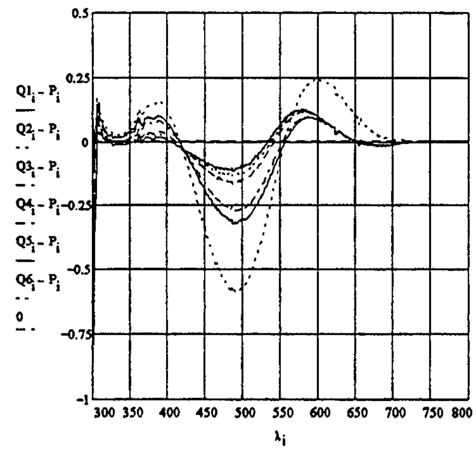

Figure 6. P = bleach film with 670nm, 25 J/cm^2 light at ~ 35°C for 40 min; Q1 =film heated at 50^{0}C for 10 min; Q3 =film heated at 50^{0}C for 25 min; Q5 =film heated at 50^{0}C for 100 min; Q6 =film heated at 50^{0}C for 11 hr 16 min.

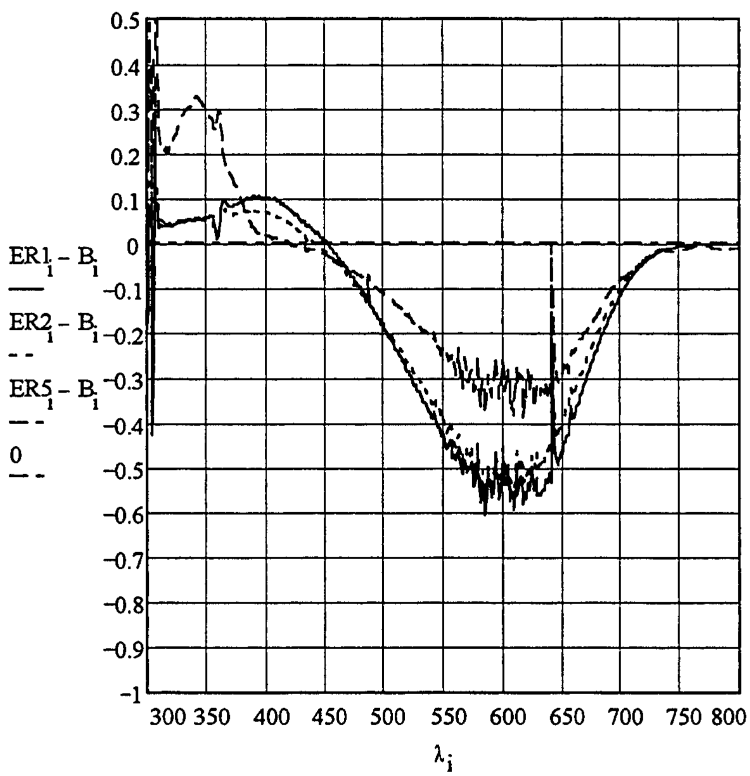

Figure 7. ER1 = erase film at room temperature with 457 nm light, 5 J/cm^2; ER2 = erase film at room temperature with 457 nm light, 12.8 J/cm^2; ER5 = erase film at approx. 45 °C, 23 J/cm^2 , pre-warm film for 20 min; B = original baseline.

3.4.2 *Blue Membrane Mutants*

The blue form of bacteriorhodopsin has a red-shifted absorption spectrum and is known to have excited state lifetimes ranging from months to years at ambient temperatures.[9,10] The red-shifted absorption makes the material compatible with existing laser diodes and the long lifetime is attractive for applications such as optical data storage or real-time holographic interferometry. The blue membrane is characterized by a ground state absorption peaked in the region of 605 nm and photoexcited states at 490 nm and 390 nm. The Q390 state has a particularly long lifetime but is formed with low efficiency.[11] The blue form occurs when aspartate-85 is neutral and can therefore be induced in wild-type by low pH or by removing the charged aspartate-85 and replacing it with a neutral residue like asparagine (N). The blue membrane shows significantly reduced optical sensitivity with respect to wild type. That is, the required optical fluence to saturate the transition (bleach or record a hologram in the material) is more than two orders of magnitude higher than required for wild type at neutral pH.[12] In this work, we have investigated a wide variety of blue membrane mutants to search for one with an improved optical sensitivity. We show that the double mutant D85N/V49A has a sensitivity that is almost two orders of magnitude better than other forms of the blue membrane. D85/V49A denotes a mutant in which two residues, aspartate (D) at position 85 and valine (V) at position 49 have been respectively replaced by asparagine (N) and alanine (A). In addition, several mutants are capable of forming the Q390-state at neutral pH.

Site-specific and random mutagenesis was used to synthesize a variety of new mutants using D85N as the wild type. Mutants were then grown in small liquid cultures (50ml) and purified by sucrose centrifugation for incorporation into a polyacrylamide gel of optical density ~1.0 in a 1 cm cuvette. Absorbance spectra were made with Shimadzu UV160U spectrophotometer and were measured as a function of exposure from a filtered white light source fitted with a 630 nm long pass filter (SRG630). The difference spectra were analyzed to detect mutants with high sensitivity and formation of the Q390 and P480 state under neutral pH conditions. Table 1 summarizes some representative mutants.

Most of the mutants had a ground state around 605 nm and a bleached state in the region of 480 nm. Several mutants including D85A, D85L and the triple D85N/A103C/G213C showed the formation of a state near 390 nm. These mutants offer the possibility of very long lifetimes; however, they were not investigated further as part of this study. Figure 8 shows the optical difference spectra for several mutants including two that formed the 390nm state.

Table 1. Summary of measured and calculated properties for the mutants forming the blue membrane that was investigated in this study.

Mutant	Ground state peak (nm)	ΔOD ground	ΔOD P480	ΔOD Q390	max. Δ*n* at wavelength ($x10^{-4}$)	Relative diffraction efficiency η	Relative bleaching efficiency
D85N	610	27 %	9 %	-	2.4 @ 680 nm	1	1
D85A	622	39 %	-	12 %	3.2 @ 660 nm	1.8	.7
D85E	610	9 %	3 %	-	0.8 @ 660 nm	0.1	.5
D85L	588	35 %	18 %	10%	2.7 @ 680 nm	1.3	1.4
D85N/D96N	575	29 %	11 %	-	2.2 @ 660 nm	0.8	1.1
D85N/V49A	610	46 %	12 %	-	4.0 @ 670 nm	2.8	7
D85N/G231C	597	34 %	15 %	-	2.8 @ 650 nm	1.4	-*
D85N/A103C/G231C	600	23 %	7 %	5 %	1.9 @ 680 nm	0.6	-*

* not measured

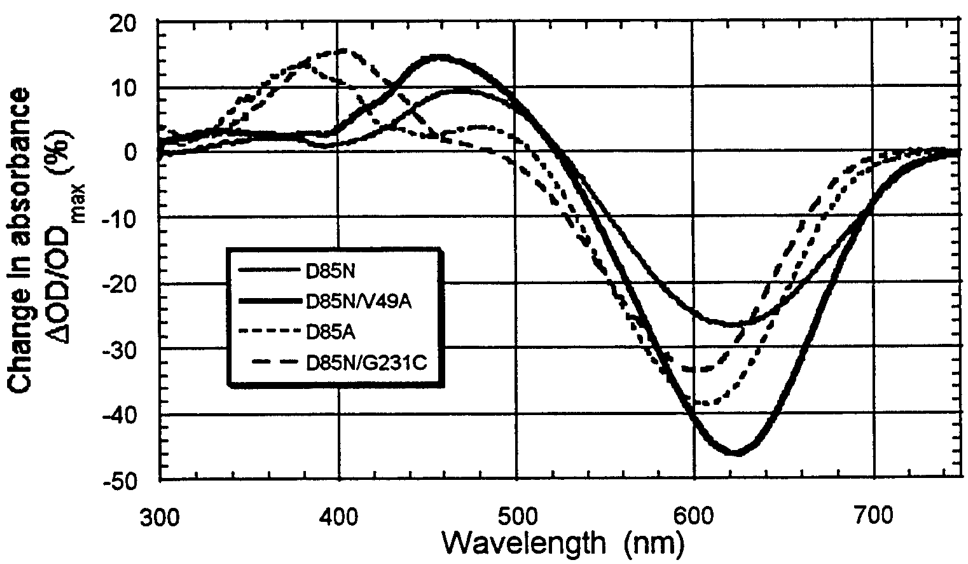

Figure 8. Measured change in absorbance after pumping with red light (>630nm) for several of the mutants investigated in this study.

The relative bleaching efficiency was determined by measuring the maximum change in optical density as a function of fluence from the filtered light source. Most of the mutants showed a similar sensitivity to D85N (within a factor of 2); however, the mutant D85N/V49A showed a significantly higher sensitivity. Figure 9 shows the measured absorption change as a function of pump beam fluence for the two mutants. The initial slope showed a factor of 7 increase over D85N.

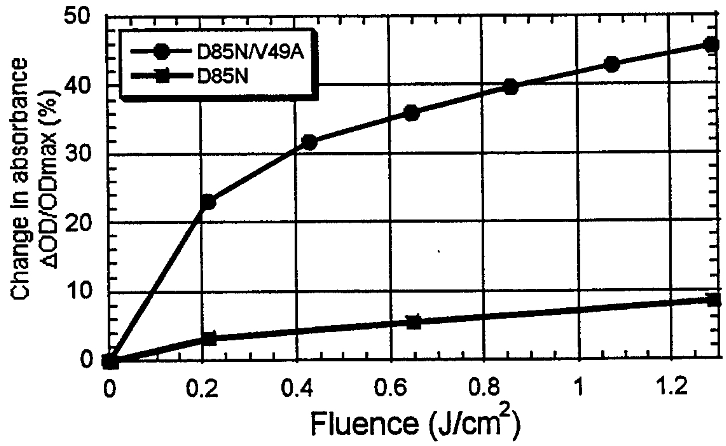

Figure 9. Measured change in absorption as a function of red light fluence for two mutants. Initial slope of D85N/V49A shows a factor of 7 increase over D85N.

To estimate the holographic efficiency of the mutants we calculated the corresponding change in refractive index, Δn from the change in absorption, Δα, using the Kramers-Kronig relations

$$\Delta n(\omega) = \frac{C_o}{\pi} P \int_0^\infty \frac{\Delta\alpha(\omega')}{\omega'^2 - \omega^2} d\omega' \quad , \tag{1}$$

where C_o denotes the vacuum speed of light and P denotes the Cauchy principal value. We performed this calculation on each of the mutants. The maximum value of Δn and the wavelength that it occurs at are listed in Table 1. To estimate holographic performance we assumed that the diffraction efficiency, η, was proportional to Δn^2, which is valid for small modulation indices. For comparison the diffraction efficiencies were normalized relative to D85N. D85N/V49A had a relative value 2.8, further indicating the potential of this material. This material is further investigated in the holographic characterization section.

3.4.3 Other 85 mutations

Several other mutations at site 85 were performed however they formed a purple rather than blue membrane at neutral pH. The results of these measurements are included in Table 2, however they were not investigated further.

Table 2. Summary of measured and calculated properties for the mutants based site 85 that formed the purple membrane.

Mutant	Ground state peak in nm	ΔOD ground	ΔOD P480	ΔOD Q390	max. Δn at wavelength	Relative diffraction efficiency η
D85S	580	11 % @ 595 nm	4 % @ 460 nm	3 % @ 370 nm	$8.2\cdot10^{-5}$ @ 671 nm	0.11
D85T	590	18 % @ 605 nm	4.3 % @ 480 nm	4.0 % @ 375 nm broad)	$1.4\cdot10^{-4}$ @ 666 nm	0.31
D85H	584	24 % @ 594 nm	7 % @ 475 nm		$2.0\cdot10^{-4}$ @ 646 nm	0.68

3.4.4 Long O-State mutants

Wayne State University performed site specific mutagenesis during this study to alter the BR and create long lived ***O***-states. Wayne State produced three long-lifetime ***O***-state materials, the mutants ***X***(E204Q), ***Y***, and ***Z***(D212N/Y185F). The mutants were produced in sufficient quantity for incorporation into films and sol-gels and were delivered to Bend Research. The mutants were characterized at UCI using a time-resolved optical multichannel analyzer. The lifetime of the D212N/Y185F mutant was found to be 100 ms, and the ***X*** mutant was approximately 7 seconds. This represents approximately a 100 fold increase over the wild type.

While the X-mutant exhibited increased ***O*** lifetime, the ***O-->P*** side reaction was not observed. Although this result was not initially understood we speculated that previous observations of the ***O --> P*** side reaction were dependent on the presence of glycerol in the films.[8] In the end the long O materials did not produce any significant results (i.e. their performance was not better than D85N and no significant branching reaction was observed even in the glycerol based films). We detail the results in the following.

The mutants X and Y and Z were tested for sensitivity of P-490 state formation in a gelatin glycerol film. The films were composed of 60% glycerol with the balance gelatin and BR. The pH of the films was 6.5. The sensitivities were monitored in a pump probe experiment with the pump laser at 676 nm and 120 mW/cm^2 and the probe laser at 633 nm. The change in the transmittance over time was normalized to OD 1. This change, which represents the sensitivity, was largest for mutant Z, followed by X and then Y. In mutant X, and to a lesser extent mutant Y, there was an initial decrease in transmittance at 633 nm, presumably due to O-640 state formation. This behavior was not seen in the Z mutant. The films were purple membrane for X and Y and blue membrane for mutant Z.

Table 3 shows the sensitivities relative to D85N. The relative sensitivity was largest for mutant Z, followed by X and then Y, although all are substantially less sensitive than D85N. Graphs of the bleaching data for shown below. The light line is the actual data of the bleaching of each mutant. The dark line is the linear fit to the data.

Table 3. Relative sensitivity of O-state mutants

	X	Y	Z	D85N
O.D.	1.1	1	0.73	0.55
Relative Sensitivity(to D85N)	0.04	.002	0.07	1

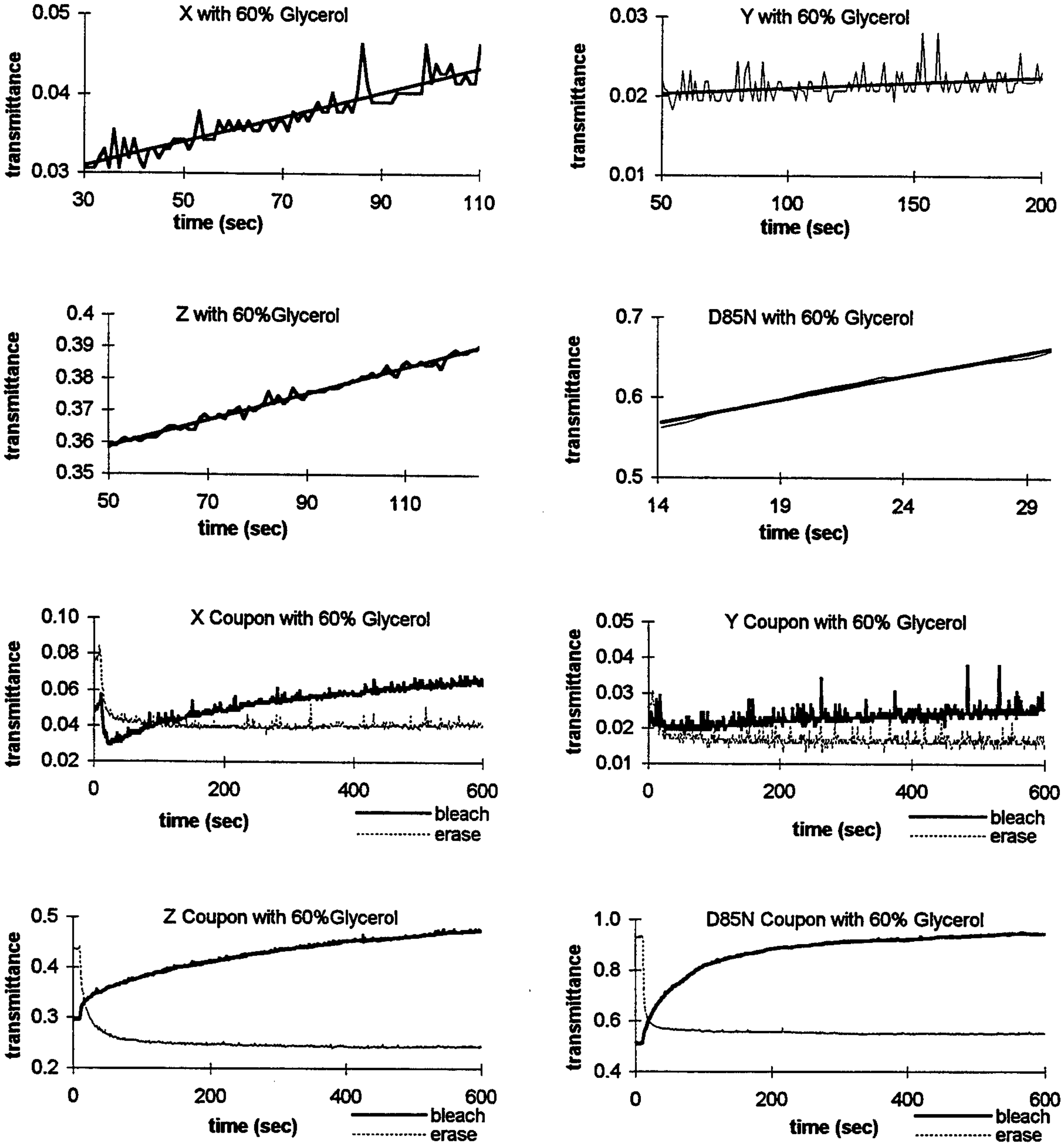

Figure 10. Transmission as a function of time for bleached samples of mutants X, Y, Z, and D85N.

3.5 Holographic Studies

Because of its outstanding sensitivity and apparent increase in refractive index modulation we selected D85N/V49A for incorporation into a gelatin film and performed holographic measurements. For comparison, an identical film of D85N was also prepared. The films were fabricated by Bend Research, Inc. and had a nominal OD of 3.5, pH = 7. Each film was 100 microns thick and had a clear aperture of at least 1 cm.

Holographic measurements were performed using a 670 nm, 10 mW laser diode. Holograms were formed by intersecting two collimated beams at an angle of 57 degrees. This resulted in a grating spacing of 0.7 microns. Diffraction efficiency was measured by periodically blocking one of the beams (the object beam) and measuring the incident, transmitted, and diffracted power. Figure 11 shows the measured dependence of output diffraction efficiency (defined as the ratio between diffracted and transmitted power) as a function of writing fluence (obtained by varying the exposure time). Bacteriorhodopsin films have been previously modeled as a saturable absorber with a saturation intensity of I_{sat}.[13] The exposure time here is much less than the excited state lifetime of these films (many days), therefore, it is more meaningful to define a saturation fluence, F_s rather than an intensity. Because the diffraction efficiency is proportional to the square of the refractive index change (for small modulation) we fit the measured data to the phenomenological model

$$\eta = \eta_0 \left(\frac{F}{F_s + F} \right)^2 , \tag{2}$$

where F is the incident fluence and η_0 is the saturated diffraction efficiency. From this fit, shown as the solid line in Figure 11, we find that the saturation fluence for D85N/V49A is approximately 50 times lower than that for D85N. This is in agreement with the sensitivity measured for absorption saturation as shown in Table 1 when the squared dependence between diffraction efficiency and the refractive index modulation is accounted for.

Although the estimated relative diffraction efficiency was a factor of 3 higher for the new mutant, the measured diffraction efficiency was approximately the same for both films (~1.5%). Small changes in the hydration and pH of the film have been shown to significantly affect on the overall diffraction efficiency.[12] Therefore, the variations in the manufacturing of the two films can partially account for this discrepancy. In addition, the non-linear response of the medium when recorded at a large intensity modulation index --reference and object beams close to 1-- results in non-sinusoidal gratings which can also account for the apparent clamping of diffraction efficiency to only a few percent.

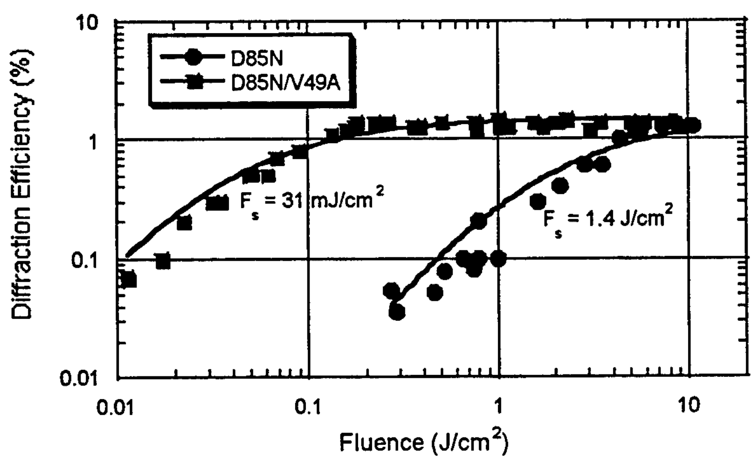

Figure 11. Measured dependence of output diffraction efficiency on writing fluence for D85N and D85N/T49A. Saturation fluences are calculated using Eqn. 2.

For grating lifetime measurements, the power in the reference beam was reduced to 50 $\mu W/cm^2$ using a neutral density filter and readings were performed periodically with a small duty cycle to avoid further bleaching of the films. Room lights were turned off during this experiment. Figure 12 shows the measured decay of a grating recorded in the new mutant film. The data showed a fast initial decay (~10 min) followed by a much slower component. An exponential fit to the longer component determined a time constant of approximately one month (660 hours). Downie, et. al.[10] showed that a diffusion-like mechanism was responsible for significantly decreasing the holographic time constant. The use of crosslinked films could help to extend the grating storage time.

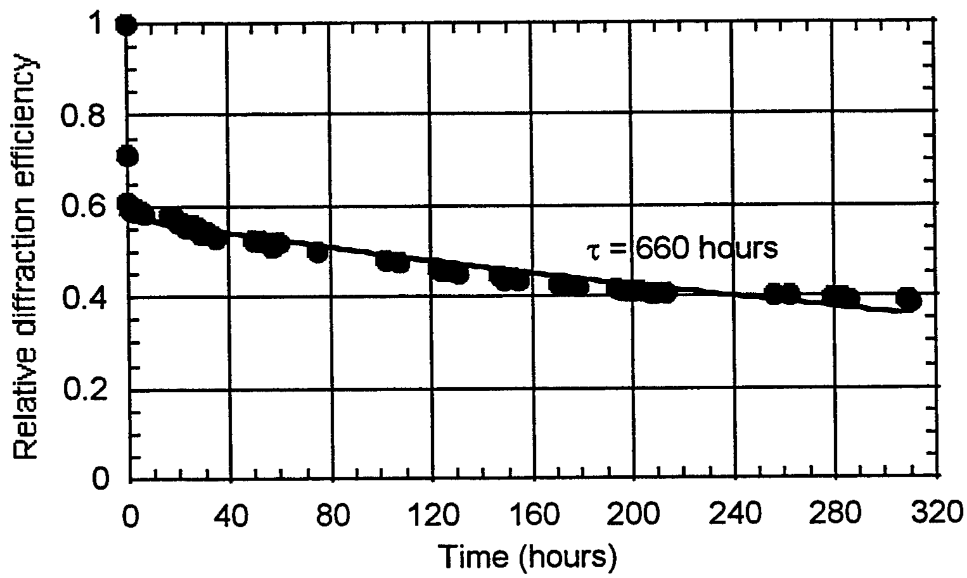

Figure 12. Measured grating lifetime in D85N/V49A film.

4. FILM PRODUCTION

4.1 Introduction

During this project, several BR-based materials, suitable for holographic storage, were manufactured. Our goal was to produce thick, high-quality BR materials for optical recording and holography. Several hosts for BR were investigated. These were sol-gel (solution-gelatin) hosts, epoxy hosts, and thick polymeric hosts. After thorough investigation, it was determined that polymer hosts were the preferred encapsulation material for BR. Our work is described in detail below.

4.2 Manufacture of BR/Sol-Gel materials

We initially investigated Sol-gel formulations due to their potential for very thick structures (>1cm). The Sol-Gel process can be used to encapsulate and/or covalently bond both organic and inorganic compounds that have large optical non-linearities. The final product can be a soft or hard gel and cast in both thin film and bulk volume forms. The Sol-Gel host results in the production of an optically thick sample that is mechanically durable, capable of being polished, and thermally stable at high temperatures.[14,15] Three types of BR were incorporated into a sol-gel matrix. These BR types are wild type and the genetically engineered strains: D96N and Y185F/D212N. All of the BR samples were prepared using a TMOS silica sol-gel process described below. The three BR strains (WT, D96N, and Y185F/D212N) were chosen based on their promise for optical applications. WT BR is known to exhibit controllable lifetimes to as long as 10 seconds and thus can be used as a real-time holographic recording material. This particular strain is also well characterized and is useful as a baseline with which to compare other BR strains. D96N BR strains are known to have very long recording lifetimes and are useful for comparative holographic interferometry and holographic data storage. Y185F/D212N is a unique BR material which has a red-shifted photochromic response (other BR strains exhibit blue-shifted responses), and is potentially useful at diode laser wavelengths for both real-time and long-lived holographic recording.

The sol-gel manufacturing process investigated during Phase I is based on the TMOS (tetra methyl ortho silicate) precursor. Other types of sol-gel precursors were investigated such as TEOS (tetra ethyl ortho silicate), methyl trimethoxy silane, dimethyl dimethoxy silane and phenyl trimethoxy silane; however, these precursors either did not gel at low temperature (temperatures which did not denature the BR) or produced poor quality materials.

The sol-gel process consists of four separate steps: 1) The formation of the sol, 2) the gelation of the sol, 3) curing of the sol-gel, and 4) drying. Each step is described separately below.

1. The first step in forming sol-gel/BR materials is the formation of the sol, or the colloidal suspension of the TMOS in water. 5.53 grams of TMOS, along with 3.3 grams of deionized water and 0.05 M of HCl catalyst is mixed and then sonicated for 25 min. Since the TMOS is not water miscible, the result is the formation of a colloidal suspension of TMOS in a water solvent. The HCl catalyst initiates the gelation upon the addition of the BR, in a pH=7 buffer,

to the TMOS. This colloidal suspension consists typically of 10 nm particles suspended in water.

2. The second step is to form the gel from the sol. This is accomplished by adding 1 mL of the desired amount of BR suspended in a pH=7.0 KPO4 buffer to 1 mL of the TMOS sol. The mixture is then thoroughly mixed and is placed in 1 cm^2 x 2 cm molds and allowed to gel, which typically takes around about 3 minutes. Gelling is the formation of Si-OH-Si bonds in such a way as to form a dense interpenetrating network with voids (absence of Si) where solvent is present. Thus, the result of gelation is the formation of a inorganic matrix surrounding the BR material. Once gelled, the material is cast into polystyrene cuvettes, sealed and placed into a refrigerator at 4° C for curing.

3. The next step, curing, takes several days to several weeks, depending upon the pH, BR concentration, and temperature of the sol-gel. Curing involves the formation of Si-O-Si bonds from Si-OH-Si bonds, which leads to the formation of a true, inorganic, glassy material containing encapsulated BR material; however, there is still a large amount of solvent (water) present which must be removed if the material is to be cut or polished.

4. Thus, the final step is to dry the BR/sol-gel material. This also must be done slowly in order to prevent cracking of the sol-gel matrix due to internal forces that are created by capillary action in the very small pores. By slowly removing water, it is possible to prevent cracking or breaking the sol-gel. Once dried, the volume of the BR/sol-gel materials is reduced by a factor of 10, which is roughly the volume of water removed.

A D96N/T46V BR/sol-gel sample with dimensions of 1cm x 1cm x 2cm was produced with a recording lifetime near 20 seconds and an optical density of 3.0 at 568 nm. This sample was placed into a polished glass cuvette of good optical quality and sealed with optical epoxy. Figure 13 shows the optical density spectra for this BR/sol-gel material. Both the initial (BR) state and the photochromic (M) state are shown. The M state was populated by exposing the sol-gel to a 500 W tungsten lamp for 3 seconds. This clearly shows that the BR is fully functional in the sol-gel matrix before drying.

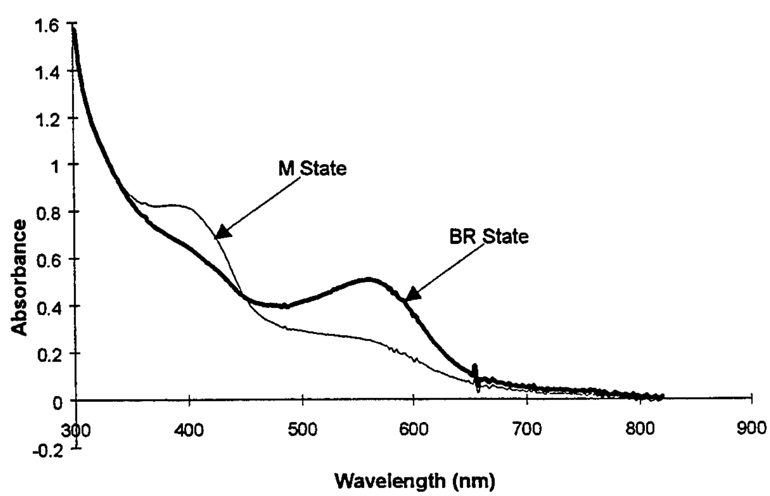

Figure 13. The absorbance spectra for a D96N/T46V BR/sol-gel sample. Increasing absorbance at short wavelength is due to the high optical scattering.

The sol-gel samples produced all have a large degree of light scattering. This is indicated by the rising absorbance for smaller wavelengths, as is shown in Figure 13. We attempted to reduce this light scattering by first sonicating the precursor with the BR included for several minutes and then gelling the solution. This produced a reasonably clear suspension; however, upon curing, the BR samples yielded additional light scattering. Thus, sol-gel materials are ultimately not acceptable hosts for BR. We therefore investigated other methods to produce thick BR materials as will now be discussed.

4.3 Manufacture of BR/Epoxy Materials

Based upon the need for better optical quality BR materials than can be achieved with sol-gels, we investigated the use of an optical epoxy as a BR host. Epoxies are desirable as hosts since they have low absorbance and light scattering and also have refractive indexes close to that of BR and glass, which can lead to refractive index matching and low optical scattering. Our initial results indicated that the resulting materials are promising as well as BR hosts. Further work will proceed to optimize the light scattering, optical density and lifetime of the BR/epoxy hosts. One benefit of such an approach is that the manufacturing of BR/epoxy materials is very simple. One simply mixes BR into the epoxy, casts the mixture onto a glass substrate (or between two glass substrates) and cures the epoxy. It may be desirable to further investigate BR/epoxy materials in a Phase II program.

4.4 Manufacture of Thick Polymeric BR Films

We also investigated polymeric hosts for BR in order to yield higher quality, thick BR materials. In fact, polymeric hosts yielded the most desirable BR materials. We initially investigated the use of polyacrylamide gels as BR hosts. We produced these gels by mixing 20 mg of BR in a 1 mL volume containing 30 % acrylamide/bis-acrylamide (in water) solution. The solution was sonicated for 1 minute to homogenize the suspension. To this solution was added 5% (by weight) of ammonium persulfate, which is a crosslinking agent (resulting in a gel). Finally, triethylene methylene diamine was added to initiate gelling. Our investigations indicated that these gels are potentially good hosts for BR. The resulting materials can be dried to a thickness approaching 1 mm with reasonably low light scattering; however, further work will need to be performed to determine the optimum film-forming conditions.

Our most successful BR materials fabrication method was to use gelatin as a polymeric host for BR. Using film-forming techniques developed over the last several years at Bend Research, we have been able to prepare 100 μm thick films of several BR materials, including the mutants D85N, D85N/V49A, D85N/D96N and D96N/T46V. All of the films exhibited long optical recording lifetimes, were of high optical quality, and form the basis of much of the optical experimentation discussed in this report. The D85N/V49A film has a recording lifetime of 27.5 days and its optical density is near 3.0 at 600 nm. The D96N/ T46V film has a recording lifetime of several hours and its optical density is near 5.0 at 570 nm.

4.5 Crosslinked films

Our latest efforts concerning crosslinking of BR materials involve the use of polymeric crosslinking agents. Polymeric crosslinkers have the advantage of being able to bridge large gaps

between reactive groups. This may be useful for dilute BR materials, i.e., where there are a small number of BR molecules per unit volume, such as is the case for thick BR materials. Polymeric crosslinkers may also better match many material properties of BR, such as having similar refractive index.

Some examples of polymeric crosslinkers include commercially available crosslinkers from Hercules, including Polycup Resins, Hercules Resins, Kymene Resins, Hercosett Resins, and Delsette Resins. These polymers have functionalities which react with secondary amines, carboxcyls, and sulfides. Amino acid side chains present in gelatin and BR which will react with these crosslinkers include amines (lysine, arginine and histidine), alcohols (hydroxyproline, threonine and serine), carboxylic acids (aspartic acid and glutamic acid), amides (asparagine and glutamine) and sulfhydril groups (cysteine). A desirable feature of these crosslinkers is that they do not become inactivated in water.

The following example demonstrates crosslinking of blue membrane materials using a polyfunctional polymeric crosslinking agent. A solution was formed by mixing 20 wt. % gelatin with 10 wt. % glycerol, 10 wt. % Kymene 557H crosslinker (Hercules, inc.) and the balance water. The solution was cast onto a glass plate and allowed to dry in room air. The BR material was then heated in an oven at 40°C to drive off more water and to increase the reaction rate. Films of crosslinked BR materials were then hydrated for 12 hours in a chamber kept at 100% humidity. No change in the absorbance spectra of the BR materials was observed after crosslinking and hydrating when compared to an un-crosslinked D85N BR film prepared under identical conditions as the crosslinked sample. The materials were then placed in a water bath at 40°C and stirred overnight. The crosslinked BR materials did not dissolve nor did the BR materials diffuse through the polymer matrix, indicating that crosslinking was achieved. Lifetime studies are in progress.

5. HOLOGRAPHIC DATA STORAGE

5.1 Introduction

Holographic data storage holds great promise as a method to achieve ultra-high data density.[16] Pages of data can be stored within a single volume of material and later an entire page can be recalled in parallel. To achieve high-density data storage it is necessary to use a multiplexing technique to permit coded storage and retrieval of data pages. A variety of multiplexing methods exist including angular,[17,18] wavelength tuning,[19,20] phase code,[21] and mechanical shifting.[22] Mechanical shifting or shift multiplexing is well suited for a disk-based architecture similar to current optical compact disks. To fully utilize shift multiplexing in a disk-based architecture it is necessary to have a holographic recording medium that can be cast as a wide area thick film.

Bacteriorhodopsin (BR) is an organic, photochromic material that has demonstrated exceptional promise as a real-time holographic material.[23,24] BR has been used in optically addressable spatial light modulators,[25,26,27] in optical correlators,[28,29,30] in phase-conjugate mirrors,[31] in optical sensors,[32] and has also found uses in optical pattern recognition[33,34,35,36] and optical computing.[37] Because it can be encapsulated in a polymer and cast as a wide area film, BR is well suited for a disk based storage system. However, naturally occurring or wild type BR has storage lifetimes on the order of a few hundred milliseconds, which is much too short to be useful for archival data storage. Through genetic engineering and careful film preparation, the optical properties of BR can be significantly modified for optimal performance in specific applications.[38] Both spectral response and storage lifetimes can be significantly altered. By extending the lifetime, BR can be used in optical memory devices.[39,40] The mutants investigated in this study, D85N and D85N/V49A, are good candidates for optical data storage because of their exceptionally long lifetime (years) and red-shifted spectral response that makes it compatible with laser diodes. The fabrication of thick films of D85N makes it useful for such applications as high-speed holographic cameras,[41] optical signal processing[42] and holographic storage.[43]

In this section we investigate the use of thick films of D85N for volume holographic memory systems. In particular, we investigate and compare the shift multiplexing properties with both spherical and speckle encoded reference beams.[22,44,45] The storage and retrieval of several holograms in a thick film of D85N using a commercial laser diode are demonstrated. We show that using speckle reference beam encoding results in a significantly higher storage density than using a spherical reference wave.

5.2 Breadboard Design

Optical elements for the data storage system were mounted on a small (30 x 46 cm^2) optical breadboard. A schematic of the system, the physical component layout, and a photograph of the breadboard are shown in Figure 14, Figure 15, and Figure 16, respectively. The coherent light source was a commercially available diode laser package with integrated current and temperature stabilization (Melles-Griot 56IMS663) operating at 692.5 nm and 22.5 mW. Its collimated output beam had a diameter of $D \approx 5$ mm. After passing through a quarter-wave plate, this beam was split into object and reference beams, the latter having a power of about 7 mW. For spherical wave shift multiplexing, a short focal-length lens was used to create a highly divergent beam

(divergence $\alpha = 18°$). The distance between the beam waist and the BR film was 19.5 mm. For speckle wave multiplexing the diverging lens was replaced with a glass diffuser. The distance between the diffuser and the BR film was z_{sp} = 30 mm which results in an average speckle size in the recording media plane of $<\varepsilon> = 1.22 \cdot (\lambda/D) z_{sp} \approx 5$ µm.

The object beam passed through a transmission type liquid crystal spatial light modulator (CyberDisplay 320 by Kopin), through a lens and then onto the BR film, where it produced a spot 1 mm in diameter. The film was placed between the Fourier and image planes. The spatial light modulator (SLM) has a resolution of 320 x 240 pixels; however, all pixels were turned off in these experiments (totally transparent mode). The optical system provided about 0.07 mW of object beam power onto the BR film. The reference beam divergence was much higher than that of the object beam at the film plane and the overlapping region corresponded to approximately 10% of the reference beam cross-section. This resulted in approximately a 10:1 intensity ratio between reference and object beams. The recording angle between object and reference beams was $2\theta \approx 62°$.

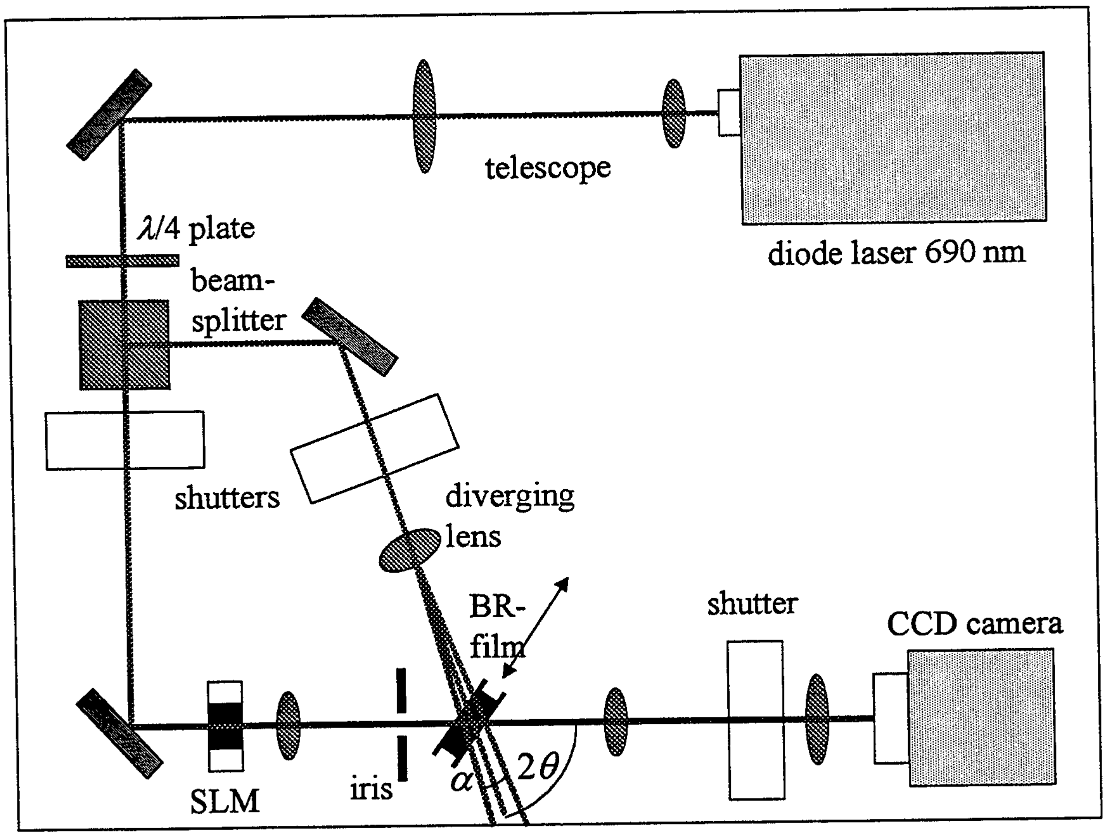

Figure 14. Schematic of the holographic data storage breadboard.

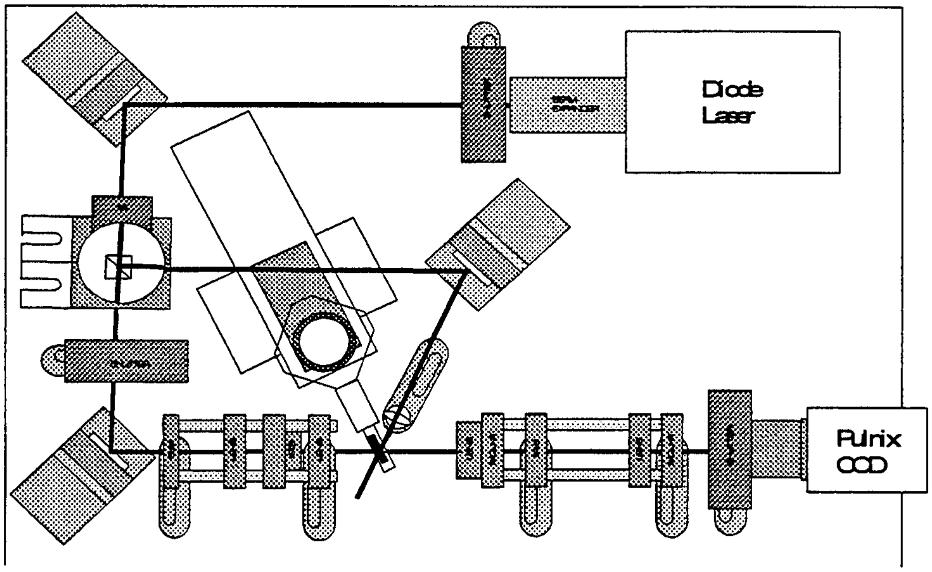

Figure 15. Physical layout of the data storage breadboard.

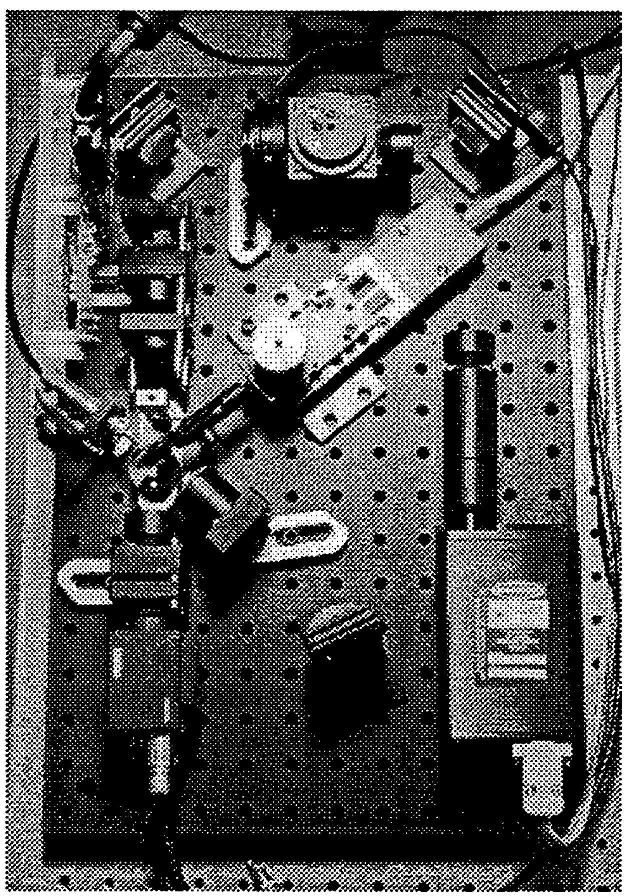

Figure 16. Photograph of data storage breadboard. Overall dimensions of breadboard is 18x13 inches.

Diffraction efficiency of the stored holograms was measured by blocking the object beam and capturing the reconstructed image with a CCD camera (PULNIX TM-7CN). The image was averaged pixelwise and normalized with a known calibration factor. This calibration factor was obtained by measuring the optical power of the diffracted beam directly with a laser power meter and relating that power to the averaged intensity of the CCD image. Furthermore, the optical power of the reference beam was also measured with the laser power meter.

Shift-multiplexing, which is the recording of several holograms within the thick film layer, was accomplished by translating the BR film in and perpendicular to the dispersion plane of the hologram with an accurate translation stage (Newport MotionMaster 2000). Shuttering of the laser beams, control of the SLM images, positioning the translation stage, image capture, and data processing was controlled by a Pentium-class PC equipped with a frame grabber card (Imagenation PX510).

5.3 Shift Multiplexing Results

A thick D85N BR film was prepared by Bend Research using a gelatin casting technique. In these experiments, the film used was about 3 mm thick and had an initial optical density ~ 3.0 at 633 nm. We recorded holograms with a total exposure of about 5 J/cm^2. The measured output diffraction efficiency (defined as the ratio between diffracted and transmitted beams) was approximately 0.7 %. Illuminating the film with filtered blue light (~ 420 nm) erased the holograms. Recording a single hologram, storing it in the dark, and periodically reading it out allowed us to estimate its lifetime. A two step decay mechanism, similar to the one described by Downie *et al.* was observed in our experiments. After an initial fast decay, a long exponential decay with a time constant of 13 days was measured, as seen in Figure 14. Absorption studies of D85N show that lifetimes of years are possible; however, a diffusion mechanism within the film leads to a more rapid decay of the holographic grating. The use of crosslinking techniques have been shown to result in stable gratings for years; therefore, in the future, it should be possible to obtain very long holographic storage lifetimes with such a material.

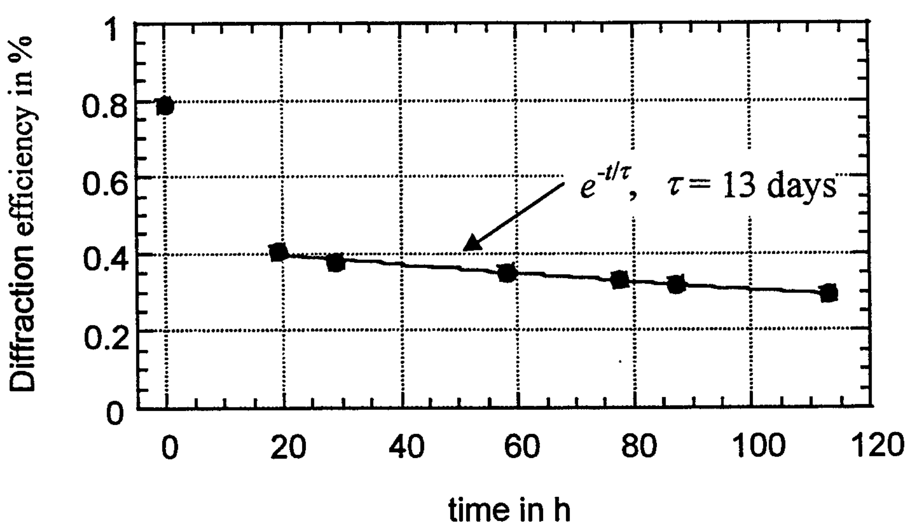

Figure 17. Measurement of the data storage lifetime of one stored hologram. A fast initial decay is followed by a slower decay with an exponential time constant of 13 days.

Shift selectivity was examined by recording a single hologram at the $(x,y) = (0,0)$ initial position of the translation stage and scanning the stage within the dispersion plane (defined as the plane that contains both recording beams). Figure 18 shows the measured diffraction efficiency as a function of shift distance for both a spherical and a speckle reference wave. For the spherical wave hologram, the full width at half maximum of the peak is 9.6 μm; however, the side-lobes occurring next to the main peak require that a larger displacement should be used between adjacent recordings to avoid crosstalk.

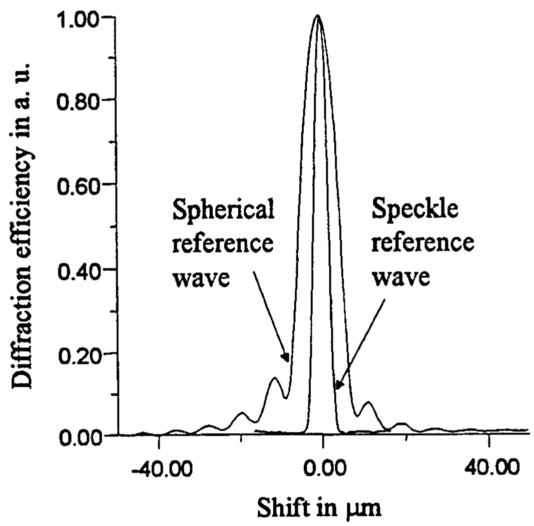

Figure 18. Measured diffraction efficiency, as a function of shift distance within the dispersion plane for a spherical and speckle reference beam. A single hologram was recorded at $x = 0$ μm. The diffraction efficiency curve is much narrower and shows no sidelobes when the hologram is recorded with a speckle reference wave.

Shift selectivity in the direction perpendicular to the dispersion plane was also measured. Figure 19 shows a surface- and contour plot of the measured diffraction efficiency of a single hologram recorded and reconstructed with a spherical reference beam at its initial position $(x,y) = (0,0)$ as function of the shift in the x- (in the dispersion plane) and y- (perpendicular to the dispersion plane) directions. It is evident that the selectivity for spherical wave shift-multiplexing is extremely asymmetric, (i.e., for shifting in the direction perpendicular to the dispersion plane, the full width at half maximum is 239 μm or 25 times larger than that for shifting within the dispersion plane.) The main mechanism of selectivity for spherical wave shift multiplexing is angular Bragg selectivity, $\delta\theta$, of the volume hologram.[22] This selectivity can be calculated as $\delta\theta \approx 2\pi/(KT)$, where T is the recording media thickness and $\boldsymbol{K}$ is the grating wave vector. The observed asymmetry is a consequence of the large difference between the recorded grating wave vectors in these two directions. The grating vector $\boldsymbol{K}_{\parallel}$ within the dispersion plane is proportional to the recording angle θ between reference and object beams, and varies as $\boldsymbol{K}_{\parallel} = 4\pi/\lambda \cdot \sin(\theta \pm \alpha)$. When the angular divergence of the spherical wave α is much less than the recording angle ($\theta >> \alpha$) the angular selectivity is dominated by the overall recording angle, $\delta\theta_{\parallel} \approx \lambda/(2\sin(\theta)T)$. The angular selectivity $\delta\theta_{\perp}$ in direction perpendicular to the dispersion plane is much lower as the corresponding grating wave vector $\boldsymbol{K}_{\perp}$ here is only a function of the spherical wave divergence, α. Moreover, the value of $\boldsymbol{K}_{\perp}$ varies significantly across the hologram, having a minimum magnitude

($K_\perp \approx 0$) along the axis of the hologram and a maximum $K_\perp = 4\pi\alpha/\lambda$ at its periphery. Because $K_\parallel >> K_\perp$ the corresponding values of the angular selectivity in these two directions strongly differ and therefore the shift selectivity for spherical wave multiplexing is asymmetric.

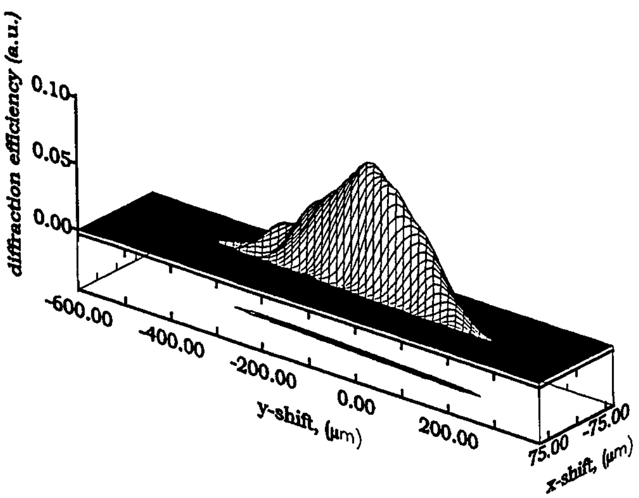

Figure 19. Measured diffraction efficiency for a single hologram recorded with a spherical reference beam as a function of the shift distance in *x*- (in the dispersion plane) and *y*- (normal to the dispersion plane) directions. Units on both axis are μm. The selectivity within the dispersion plane is much higher.

Shift selectivity using a speckle reference wave was examined in a similar way as in the case of a spherical reference wave. Figure 18 illustrates the measured intensity of the diffracted beam as a function of the displacement in the dispersion plane. Two characteristics of the plot are noteworthy. First of all, the speckle shift selectivity curve $\eta(x,y)$ is substantially narrower (2.6 times) than that of the spherical wave shift selectivity measured under similar conditions. The measured value of the speckle shift selectivity of 3.7 μm is close to the average speckle size $<\varepsilon> \approx$ 5 μm in this direction. The second feature of the speckle wave curve in Figure 18 is the absence of sidelobes around the main peak, which is unlike the situation for spherical wave shift multiplexing.

It was demonstrated[44] that the main mechanism of shift selectivity for a speckle encoded reference beam volume hologram is due to spatial de-correlation between recorded and reconstructing speckle structures in the lateral direction and is independent of the grating period. As the shift value becomes larger than the average lateral speckle size $<\varepsilon>$ the diffracted beam intensity drops rapidly to zero. Furthermore, the correlation function for a speckle pattern with Gaussian statistics (average speckle size $<\varepsilon(x,y)>$) is a symmetric function in both lateral directions, and therefore the shift selectivity of the volume hologram is symmetric in the *x*- and *y*- directions. A 2-D surface-plot and contour map of the shift selectivity measured for a single speckle reference wave hologram recorded at $(x,y) = (0,0)$ and reconstructed using the same speckle reference beam is shown in Figure 20. To measure this plot, the translation stage was scanned sequentially over the (x,y) coordinates. The plots show that the shift selectivity is the same for both the *x*- and *y*- directions. The differences between selectivity for the case of a spherical reference beam and a speckle reference beam are summarized in Table 4.

Table 4. Measured shift selectivity for the case of a speckle and spherical wave reference beam expressed as the full width at half maximum of the diffraction efficiency signal for a single hologram.

	In the dispersion plane	Perpendicular to the dispersion plane
Spherical wave shift multiplexing	9.6 μm	239 μm
Speckle wave shift multiplexing	3.7 μm	3.7 μm

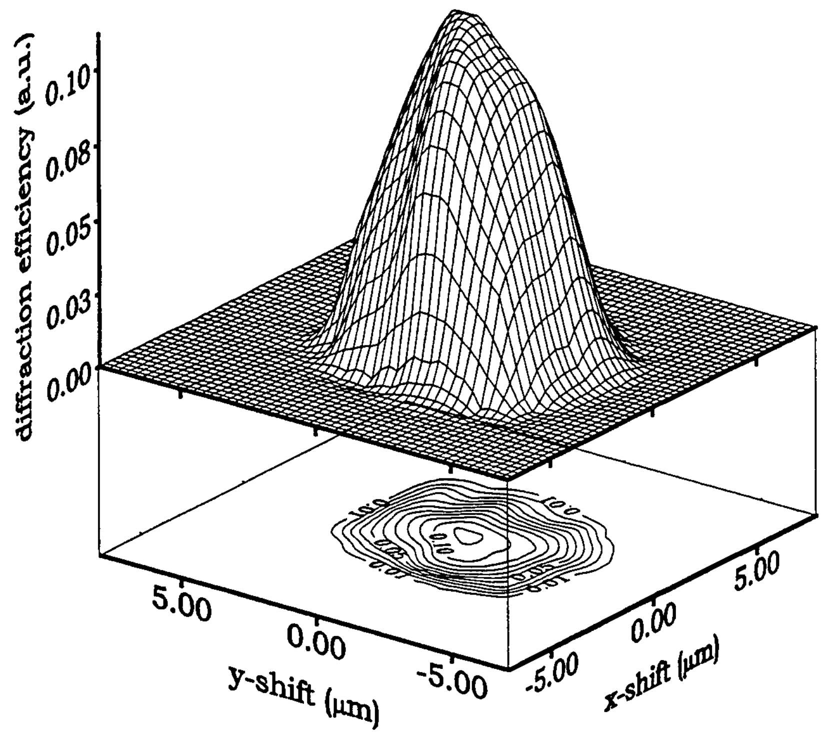

Figure 20. Measured diffraction efficiency for a single hologram recorded with a speckle reference beam as a function of shift distance in *x*- (in the dispersion plane) and *y*- (perpendicular to the dispersion plane) directions. Units on both axes are μm.

Figure 21 shows the result of sequential retrieval of three recorded holograms using the speckle multiplexing technique. The relative positions of the translation stage at recording and reconstruction were -5.5 μm, 0 μm, and 5.5 μm, respectively. The peaks are well resolved, but spaced much closer than spherical wave multiplexing would allow.

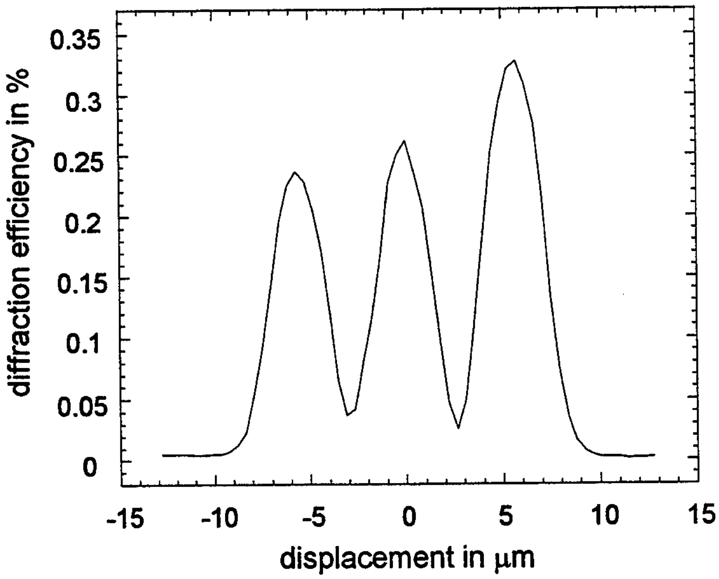

Figure 21. Measured diffraction efficiency as a function of shift distance for three holograms recorded with a speckle reference wave at x = -5.5 μm, 0 μm, and 5.5 μm in a 3 mm D85N film.

5.4 Digital Data Storage

The recording and playback of data from the breadboard were automated using a PC. The PC controlled the image sent to the SLM, shuttering of the lasers, timing of the exposures, positioning of the film, capture of the reconstructed image, and analysis of the data. Figure 22 shows the graphic user interface that was written in Visual Basic to control the read/write process. An output string can be typed into the text area (in this case it is some lines of code from the computer program itself). The string is then converted into a digital pixel sequence. The first column and first eight rows of pixels correspond to the 8 bit ASCII code for the first letter of the string. The next letter is coded into the second column and 8 rows. For example:

```
string: A s   S
        | | | |
output: 0 1 1 0
        0 0 0 0
        1 0 1 0
        0 1 1 0
        0 0 0 0
        0 1 1 1
        1 1 1 1
        0 0 0 0
```

The pattern repeats until the last column is reached at which point it increments to the first column, rows 9-16.

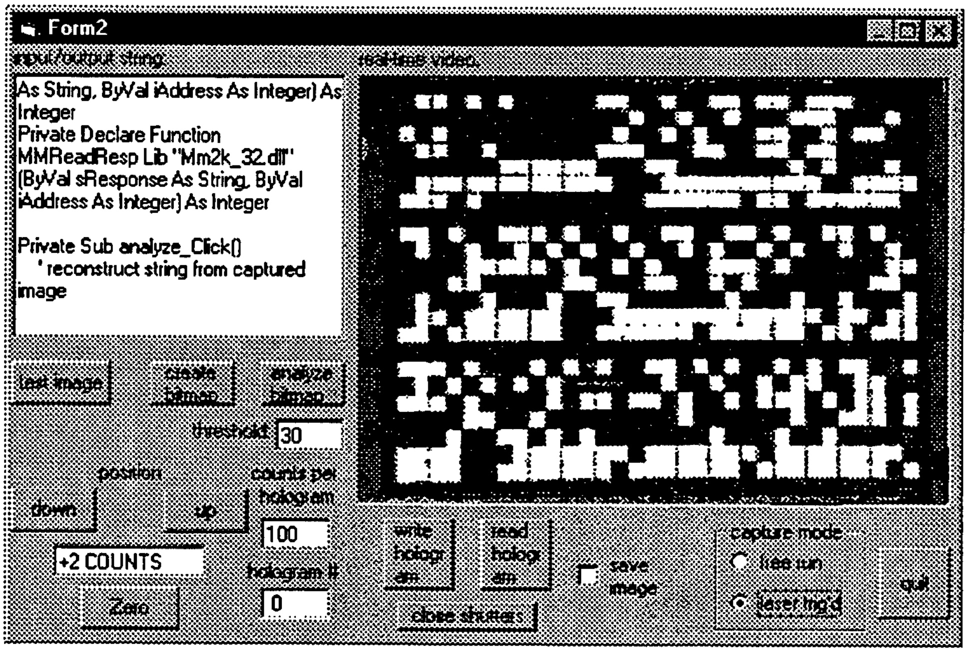

Figure 22. Graphical interface for controlling recording and readout of digital images.

Figure 23 shows a reconstructed holographic image from a D85N film. Although the pixels are clearly resolved, there is some non-uniformity within each pixel. This is partly a result of using optics on hand rather than selecting optimized components. We are currently in the process of obtaining an improved set of optics. The other element that degrades image quality is the BR film itself. Bend Research is addressing issues of film uniformity in their next generation of films.

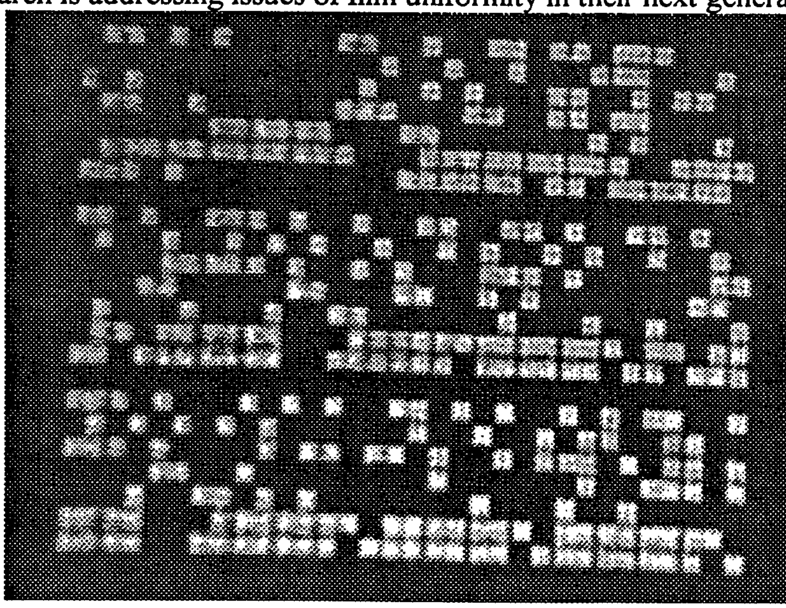

Figure 23. Reconstructed holographic image of digital data.

```
Input text string:

Dim a(100000)
Public mm2k_Addr As Integer
Public number As Integer
Private Declare Function M
Reconstructed and decoded text:

Dim a(100000)
Public mm2k_Addr As Integer
Public number As Integer
Private Declare Function M
```

The pixel quality was evaluated by sampling the brightness of several random pixels and plotting a histogram of the results (Figure 24). The histogram shows a large separation between the ones and zeros in the image. A large separation between each peak and small width of each distribution corresponds to a large signal-to-noise ratio and small bit error rate.

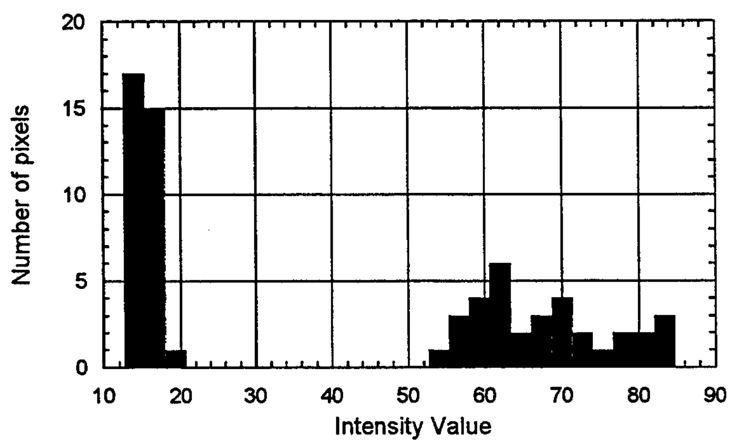

Figure 24. Histogram of selected pixels from reconstructed holographic image. Histogram indicates a good signal-to-noise ratio for the stored data.

5.5 Performance Estimates

The storage capacity of this holographic memory system can be estimated by assuming a bit-density of 76,000 bits per hologram (SLM resolution 320 x 240 pixels), using speckle wave multiplexing with 10 μm shift between holograms (thickness of the recording material is 3 mm), and a recording area of 9500 mm^2 (typical surface area of a CD-ROM). A theoretical capacity of $7.3 \cdot 10^{12}$ bits (7.3 Tbit) or $9 \cdot 10^{11}$ bytes (.9 Tbyte) results. This is over 1,400 times larger than the capacity offered by today's CD-ROMs. The ultimate storage density (capacity) will be limited by scattering and saturated index change in the material. Tests showed that with the BR materials available to us we were able to store about 20 holograms (each with 76000 data bits) into a spot of about 1 mm^2 and still obtain a diffracted signal above the scattered noise level. This results in a storage capacity of 1.8 Gbyte for a CD-ROM sized disk which is considerably smaller than the theoretical limit. With improved manufacturing techniques aimed at reducing scattered light in the film, the storage capacity can be increased towards the theoretical limit.

6. HOLOGRAPHIC INTERFEROMETRY SYSTEM

6.1 Introduction

Holographic interferometry was first applied to flow visualization over 30 years ago[46,47]. Since that time, despite numerous technological innovations, the technique has seen limited use in flow research. There are many reasons for this including the expense of the necessary hardware, tedious darkroom processing, the difficulty in aligning the optical system, and the difficulty in obtaining quantitative results. Also, the increasing reliance on computational fluid dynamics (CFD) has reduced the usage of laboratory flow visualization. The novel holographic interferometer described here successfully circumvents most of the difficulties that have plagued so many holographic interferometers in the past, provides visualization of transient phenomena that is not accurately modeled by CFD, and can provide CFD code validation.

In real-time holographic interferometry (RTHI), a holographically recorded object wave that passed through a static test field (no flow) is interfered with a real-time object wave passing through the test field while the flow is on. There are several advantages RTHI systems have over conventional interferometers, such as a Mach-Zender interferometer. Optical alignment is much simpler with a RTHI system and since most optical aberrations cancel, inexpensive optics can be used. In the past, the use of RTHI was difficult because of the inadequacies of the available recording materials. Silver halide emulsions require darkroom processing and if removed from the recording setup, must be replaced precisely in their original location or numerous unwanted fringes result. In an effort to minimize plate movement, liquid gates have been used to develop the plates *in situ*[48]. Photorefractive crystals, which are reusable and require no darkroom processing, have been used in RTHI systems with some success[49,50]. The main disadvantages of photorefractive crystals are that the crystals are expensive and their small size limits resolution and makes them difficult to work with. In this work we use a recently developed variety of the photochromic recording material Bacteriorhodopsin (BR). Previously reported varieties of BR used in holographic interferometers[51] lacked the storage time necessary for a RTHI system. A new variety based on the mutant D85N exhibits long storage times (days) making it ideal for RTHI. Unlike the photographic plates typically used in holographic interferometry, BR requires no dark room processing. BR films can be recorded and erased thousands of times without noticeable degradation, and have a spatial resolution greater than 2000 lines/mm. A BR hologram is easily erased with a filtered white light source. BR can also be fabricated into large films unlike photorefractive crystals. In this research we utilized two varieties of the BR recording material, a blue film with storage times of many days and sensitivity out to 700 nm, and a purple film with storage times of minutes and sensitivity in the green spectral region.

6.2 High Speed or Time-Differential Holographic Interferometry

Visualization of transient phenomenon is important for understanding and modeling the onset of turbulent flow. Because transient bursts are typically characterized by weak (sub-fringe) events, it is important to remove the often high-density fringes due to the steady-state flow. By interfering two holographic images that are recorded close in time, it is possible to eliminate all background or steady state fringes and view only the component of the flow that has changed during the time between pulses. A single silver halide plate is typically used to record the two superimposed

holograms. After exposure, a new plate must be inserted before the next recording and the interferogram cannot be viewed until the plate has been processed[52]. Digital holographic methods have been used in high-speed holographic interferometers[53]; however the large pulsed laser and high-resolution digital camera required make the system expensive and the resolution is not as good as film. The use of BR recording materials with short storage lifetimes enables the interferogram to be viewed immediately and the data collection rate is limited only by the time required to erase the previous hologram (~ 1 s).

6.3 RTHI Experiment

Our first experiment was to demonstrate a BR-based, real-time holographic interferometer using the long storage blue film. Figure 25 is a diagram of the optical setup. A 10 mW HeNe laser was used to record the 'no-flow' or baseline hologram in the blue BR film. A 25 mW HeCd laser was used as an erasure source, however a filtered white light source was found to work sufficiently in later experiments. During exposure, the shutters in front of the CCD camera and the erase beam were closed. After the proper exposure time (100 s for 10 mW), an attenuator was placed in the object beam (OD 3) and the shutter in front of the CCD camera was opened. The reference beam reconstructed the holographically stored baseline object beam, which then interfered with the attenuated real-time object beam. Any changes to the phase of the object beam resulted in a real-time interference pattern that was recorded by a CCD camera.

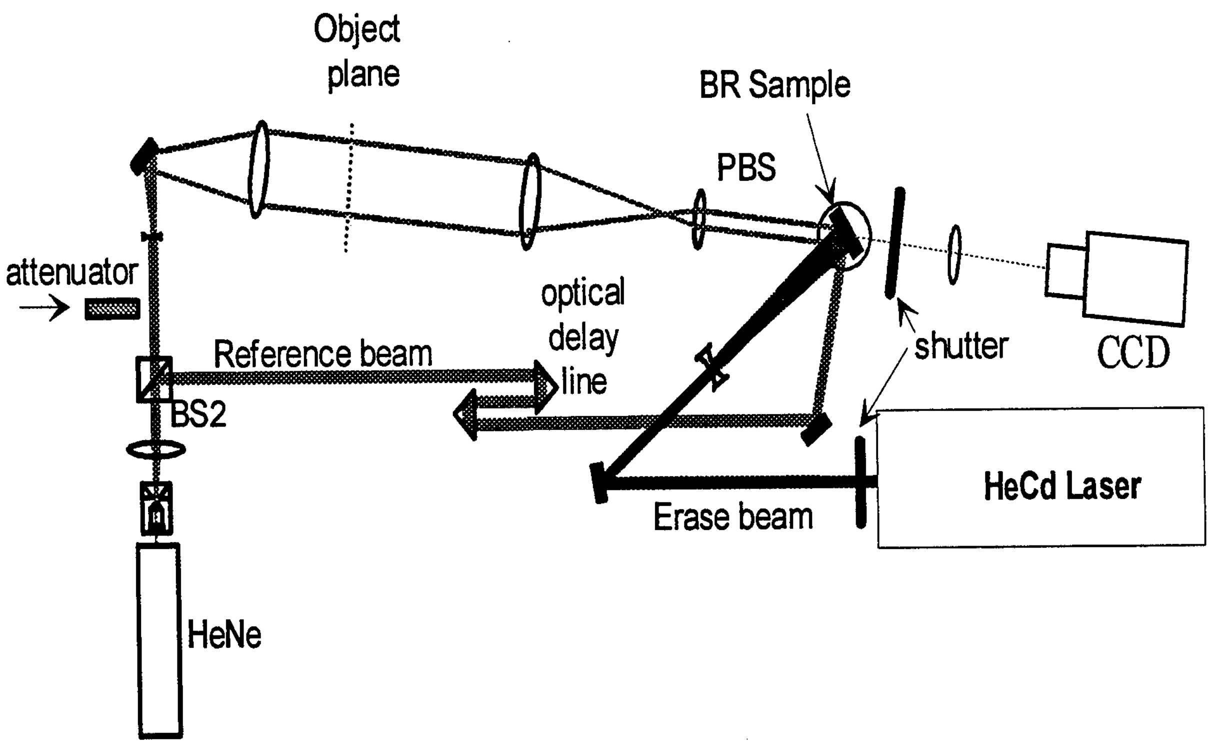

Figure 25. Diagram of real-time holographic interferometer breadboard.

Figure 26 shows several of the interferograms captured with the real-time system. High contrast interferograms could be produced for hours from a single baseline recording. Finite-fringe interferograms were produced by slightly tilting one of the mirrors in the object beam. We

recorded interferograms of flow fields generated from an air jet nozzle (Figure 26a and b), a flow field around a curved surface (Figure 26 c), thermal gradients produced by a flame (Figure 26d), and optical components such as glass plates (not shown). The full utility of the interferometer can best be appreciated by viewing the real-time nature of the playback process and the rapid erasure and re-exposure of the baseline hologram.

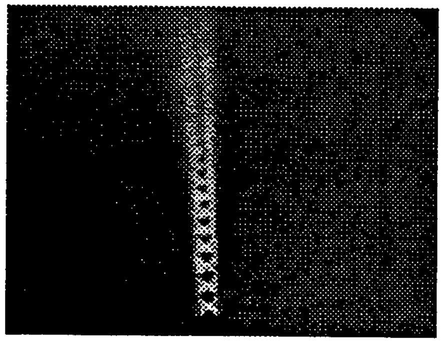

a)

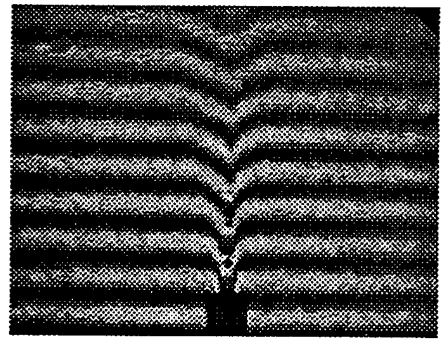

b)

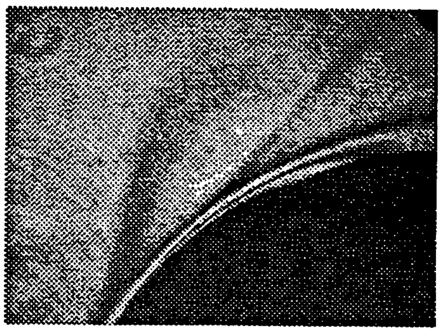

c)

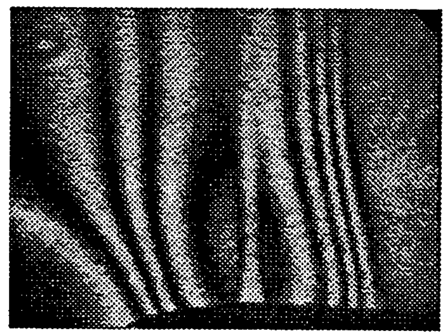

d)

Figure 26. Real-time holographic interferograms of flow fields. a) and b): Finite and infinite fringe interferograms of air flow from a nozzle. c) Infinite fringe interferogram of air flow around a smooth curved surface. d) Infinite fringe interferogram of a butane flame.

6.4 High-Speed Holographic Interferometry Experiment

In a second experiment we demonstrated a high-speed, or time-differential holographic interferometer that records a hologram with a single 8 ns laser pulse on a purple BR film. Single shot holographic images can be viewed directly or interfered with subsequent frames for purposes of capturing high-speed events. The optical setup shown in Figure 25 was modified by using a pulsed laser to record the holograms and a HeNe laser to reconstruct the images so that data could be readout between laser pulses. For simplicity, we used consecutive pulses from our 10 Hz pulsed dye laser to record two holograms 100 ms apart. Several commercially available YAG lasers are capable of generating two laser pulses with an adjustable temporal separation as small as several microseconds.

Figure 27 shows a time differential interferogram of the same flame source imaged in Figure 26d. The interferogram was produced instantaneously by reconstructing and interfering the wavefronts from two superimposed holograms recorded 100 ms apart. Note that in comparison with Figure 26d, only the turbulent inner cone of the flame is visible. The background subtraction feature

permits only time varying flow features to be recorded. This type of system is useful for imaging turbulence or other unsteady flow phenomenon. The single shot measurement capability demonstrates the ability to construct a high-speed holographic camera system for recording extremely fast events.

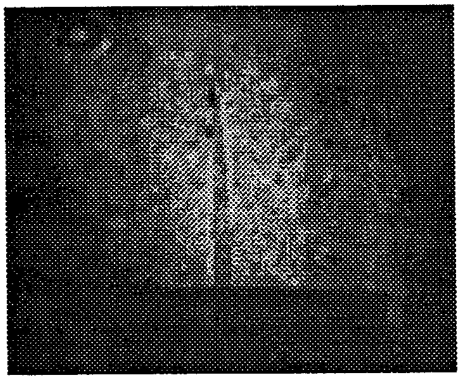

Figure 27. Reconstructed holographic interferogram of a flame recorded by two pulses separated by 100 ms. Single-shot recording demonstrates potential for a high-speed holographic camera system.

6.5 Data Reduction

Phase Shift Interferometry (PSI) is the most established technique for recovering the phase from an interferogram and is capable of resolutions greater than $\lambda/200$[54]. Typically, four interferograms must be acquired with a phase shift between each interferogram before any change in the flow field occurs. A piezo-electric actuated mirror can be used to introduce the reference wave phase-shifts necessary to perform PSI; however, obtaining four interferograms sequentially can be difficult with rapidly changing flows. A novel method is reported here for generating multiple phase-shifted images simultaneously (patent pending). The method is based on the instantaneous phase measurement technique described by Smythe and Moore[55], but uses a Holographic Optical Element (HOE) and a quadrant phase retardation mask for a compact, single CCD camera system. The novel instantaneous phase measurement method, shown in Figure 28, requires that the reference and object beams be exactly superimposed and orthogonally polarized. The HOE is used to split the combined beam into four separate beams. Each beam is given a discrete phase shift by a quadrant phase retardation mask constructed from polarization optical components as shown in Figure 28. The four phase-shifted interferograms are then imaged onto a CCD camera.

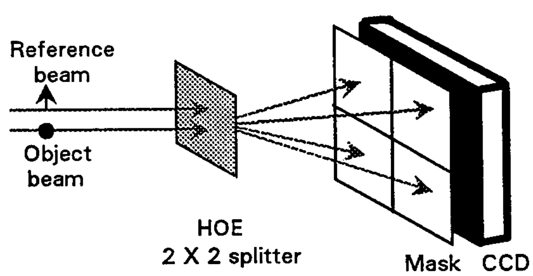

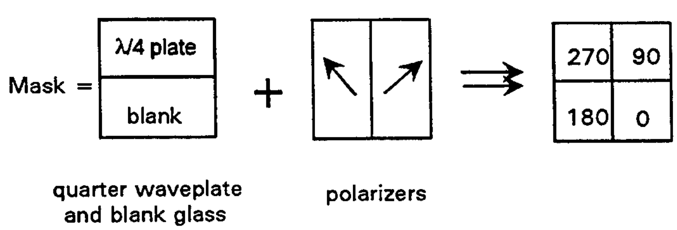

Figure 28. Novel instantaneous phase measuring technique.

The full breadboard implementation of an RTHI system using this data reduction method is shown in Figure 29. Software was written to acquire, analyze and display the phase maps. The direct phase calculation algorithm is based on a single frame of data and calculates phase according to

$$\Phi(x,y) = \tan^{-1}\left(\frac{I_3(x,y) - I_1(x,y)}{I_0(x,y) - I_2(x,y)}\right), \tag{3}$$

where, I_0, I_1, I_2, and I_3 are the sub-images from the four quadrants of the camera and x, y are the pixel coordinates. To reduce errors due to noise in the image, a form of spatial averaging can be used to smooth the phase map while still retaining a sharp transition at the 2π - 0 phase step. The spatially averaged phase is calculated using a method similar to that proposed by Hong *et. al*[56]. Using this method

$$\Phi(x,y) = \tan^{-1}\left(\frac{\sum\limits_{x,y\in\delta}\left(I_3(x,y) - I_1(x,y)\right)}{\sum\limits_{x,y\in\delta}\left(I_0(x,y) - I_2(x,y)\right)}\right), \tag{4}$$

where the sums are performed over the range of δ nearest neighbors. Increasing the number of averaged pixels improves smoothness of the phase map at the expense of spatial resolution; however, the sharpness of the phase discontinuity is retained permitting rapid phase unwrapping.

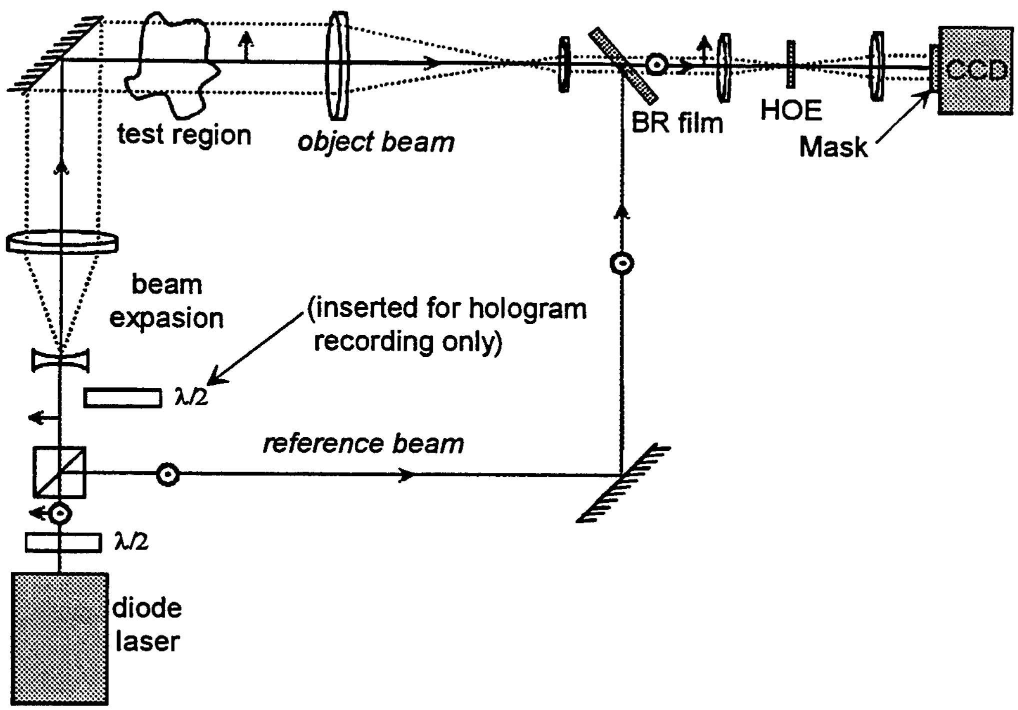

Figure 29. Optical diagram of RTHI system using the instantaneous phase measurement technique.

Four phase-shifted interferograms of an air jet flow using this method are shown in Figure 30. Figure 31 is the wrapped phase map produced from the interferograms shown in Figure 30. Figure 32 is an unwrapped phase map of the air jet flow.

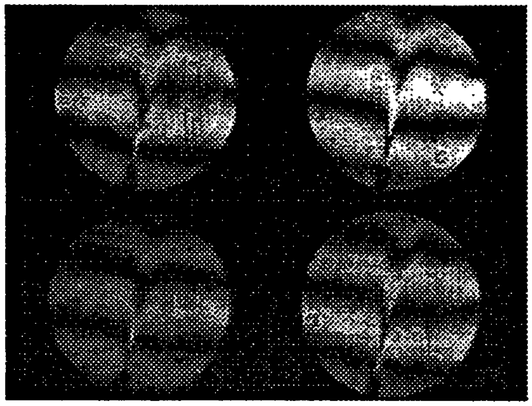

Figure 30. Four phase-shifted images of air jet imaged on to a single CCD.

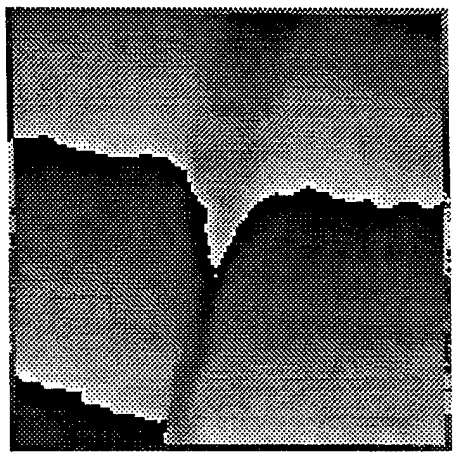

Figure 31. Wrapped phase maps of air jet obtained using the real-time interferometer and PSI software.

Figure 32. Unwrapped phase map of air jet flow obtained with PSI software.

The image phase shift can be related to the fluid density using the following relation[57],

$$\phi = \frac{2\pi}{\lambda} \int \sum_i K_i \rho_i d\ell , \tag{5}$$

where λ is the wavelength, the line-of-sight integration increment is $d\ell$, K_i and ρ_i are, respectively, the Gladstone Dale constants and the partial densities of the individual gases present.

6.6 Flow Facility Integration

Since much of the hardware required by the real-time holographic interferometer is commonly found in flow research facilities (*i.e.* Schlieren mirrors, laser, and CCD camera), a quantitative flow visualization system can be constructed inexpensively. The data acquisition rate is limited only by the camera framing-rate, since the four phase-shifted interferograms are recorded simultaneously. For pulsed facilities, the RTHI system could be integrated with a high-speed film camera. The developed film could then be digitized and processed by the PSI software to obtain quantitative data. The low cost of the system and its real-time recording ability enable it to be used as a flow monitoring system to assist with troubleshooting flow problems and data anomalies in addition to acquiring quantitative data.

7. CONCLUSIONS

In conclusion, we have synthesized and measured the optical absorption properties of several mutants bearing properties similar to the blue membrane. Several mutants were identified that form the so-called "Q390 state" at neutral pH, although the ultra-long storage lifetime of this state was not investigated. The double mutant D85N/V49A showed a factor of 50 increase in holographic recording sensitivity compared with the single mutant D85N, and had a similar diffraction efficiency. The increased sensitivity of this mutant in the spectral range of laser diodes and its long storage lifetime makes this film a good choice for real-time holographic interferometry systems and optical data storage applications.

We demonstrated that a compact diode laser can be used to record and reconstruct holograms in thick films of the mutant BR D85N. It was demonstrated that long data storage lifetimes (several weeks) can be achieved. An internal diffusion process limits the lifetimes; however, use of cross-linked BR materials could substantially increase the data storage time. High data densities were achieved using shift multiplexing. It was demonstrated that the use of a speckle wave reference beam results in a much higher storage density than the use of a spherical reference wave. Spherical wave shift multiplexing was shown to have a highly asymmetric selectivity in the directions within and normal to the dispersion plane while the speckle wave reference beam shift selectivity was shown to be equal in both directions. Furthermore, the holograms recorded with a speckle wave reference beam were shown to have suppressed sidelobes compared with spherical wave holograms. These differences lead to reduced crosstalk between stored holograms and permit an increase in storage density by over two orders of magnitude. With improved materials (reduced scattering, crosslinked polymer host) and the use of a high-resolution SLM (1248 x 1024 pixels) to write data pages, a 3 mm thick, CD-ROM sized disk of D85N could potentially be used to store hundreds of Gbytes of information.

Finally, we described and demonstrated a BR-based, real-time holographic interferometer system. The simplicity, versatility and quantitative capability make it ideal for flow visualization research. The novel instantaneous phase measurement method enables quantitative results to be produced immediately.

8. REFERENCES:

[1] R.R. Birge, "Protein Based Computers" *Scientific American*, pp. 90-95, March (1995).

[2] D. Oesterhelt, C. Brauchle and N. Hampp, "Bacteriorhodopsin: a biological material for information processing" *Quarterly Review, Biophysics*, 24, p. 425, (1991).

[3] C. Brauchle, N. Hampp and D. Oesterhelt, "Optical Applications of Bacteriorhodopsin and its Mutated Variants", *Adv. Mat.* 3, 420 (1991).

[4] A. Hafiz, R. Magnusson, J.S. Bagby, D.R. Wilson, and T.D. Black, "Visualization of aerodynamic flowfields using photorefractive crystals" *Appl. Opt.* **28**, p. 1521 (1989).

[5] F.H. Mok, "Angle-multiplexed storage of 5000 holograms in lithium niobate", *Opt. Lett.* **18**, p. 915 (1993).

[6] S. Wu, L.M. Ellerby, J.S. Cohan, B. Dunn, M.A. El-Sayed, J.S. Valentine and J.I. Zink, "Bacteriorhodopsin Encapsulated in Transparent Sol-Gel Glass: A New Biomaterial" *Chem. Mat.* 5, p. 115 (1993).

[7] M. Krebs and H. Khorana, *"Mechanism of light-dependent proton translocation by bacteriorhodopsin,"* *J. Bacteriology*, 175, pp. 1555-1560 (1993).

[8] A. Popp, M. Wolperdinger, N. Hampp, C. Brauchle, and D. Oesterhelt, "Photochemical conversion of the O-intermediate to 9-cis-retinal containing products in Bacteriorhodopsin films." *Biophysical Journal*, Vol. 65, pp. 1449-1459 (1993).

[9] J. Tallent, Q. W. Song, Z. Li, J. Stuart, and R. R. Birge, "Effective photochromic nonlinearity of dried blue-membrane bacteriorhodopsin films," *Opt. Lett.* Vol. 21, no. 17 pp. 1339-1341 (1996).

[10] J. Downie, D. Timucin, Dan Smithey, and M. Crew, "Long holographic lifetimes in bacteriorhodopsin films," *Opt. Lett*, Vol. 23 no. 9 pp. 730-732 (1998).

[11] A. Popp, M. Wolperdinger, N. Hampp, C. Brauchle, and D. Oesterhelt, "Photochemical conversion of the O-intermediate to 9-cis retinal containing products in Bacteriorhodopsin films," *BioPhys. J.* Vol. 65 pp. 1449-1459 (1993).

[12] J. Downie, D. Smithey, "Measurements of holographic properties of bacteriorhodopsin films," *Applied Optics*, (1995).

[13] A. Peda'el, R.Daisy, M. Horowitz and B. Fischer, "Beam-coupling induced transparency in a bacteriorhodopsin-based saturable absorber," *Opt. Lett.* Vol. 23 no. 15 pp. 1173-1175 (1998).

[14] H. Weetall, "D96N Mutant Bacteriorhodopsin Immobilized in Sol-Gel Glass Characterization," *Appl. Biochem. and Biotech.*, **49**, p. 241 (1994).

[15] R. Johnson and A. Tanguay, Jr. "Stratified volume holographic optical elements" *Opt. Lett.*, **13**, 189 (1988).

[16] IBM Holographic Optical Storage Team, "Holographic storage promises high data density." *Laser Focus World*, November 1996.

[17] G. Nordin and P. Asthana, "Achieving a minimum signal-to-noise ratio in angularly multiplexed volume holographic optical data storage systems." *SPIE* **2297**, p. 392 (1994).

[18] F. H. Mok, "Angle-multiplexed storage of 5000 holograms in lithium niobate." *Opt. Lett.* **18**, 915 (1993).

[19] G. A. Rakulich, V. Leyva, and A. Yariv, "Optical data storage by using orthogonal wavelength-multiplexed volume holograms." *Opt. Lett.* **17**, 1471 (1992).

[20] K. Curtis, C. Gu, and D. Psaltis, "Cross talk in wavelength multiplexed holographic memories." *Opt. Lett.* **18**, 1001 (1993).

[21] C. Alves, G. Pauliat, and Gérard Roosen, "Dynamic phase-encoding storage of 64 images in a $BaTiO_3$ photorefractive crystal." *Opt. Lett.* **19**, 1894 (1994).

[22] D. Psaltis, M. Levene, A. Pu, and G. Barbastathis, "Holographic storage using shift multiplexing." *Opt. Lett.* **20**, 782 (1995).

[23] R. R. Birge, "Protein Based Computers" *Scientific American* **272**, 90 (1995).

[24] D. Oesterhelt, C. Bräuchle, and N. Hampp, "Bacteriorhodopsin: a biological material for information processing", *Biophysics* **24**, 425 (1991).

[25] J. D. De-la-Llave, D. A. Pommet, and M. A. Fiddy, "Novel joint transform correlator architecture using bacteriorhodopsin optically addressable spatial light modulators", *Optical Engineering* **37**, 27 (1998).

[26] L. R. Lindvold, H. Lausen, "Projection display based on an optically addressed spatial light modulator using a bacteriorhodopsin thin film as a photochromic material", *SPIE* **3013**, 202 (1997).

[27] H. Takei and N. Shimizu, "Spatial light modulation based on photo-induced change in the complex refractive index of bacteriorhodopsin", *Appl. Opt.* **35** 1848 (1996).

[28] D.Y. Zang, J.E. Millerd, D. Smithey, "Asymmetric, reflection mode nonlinear Fabry-Perot modulator using bacteriorhodopsin", *Appl. Phys. Lett.* **69**, 3143 (1998).

[29] D. Sanchez, D.A. Pommet, and M.A. Fiddy, "Compact optical correlator for machine vision with optically addressed bacteriorhodopsin spatial light modulator", *SPIE* **2908** 198 (1996).

[30] R. Thoma and N. Hampp, "Adaptive bacteriorhodopsin-based holographic correlator for speed measurement of randomly moving three-dimensional objects", *Opt. Lett.* **19** 1364 (1994).

[31] D. Zeisel and N. Hampp, "Dynamic self-pumped phase-conjugating mirror based on the bacteriorhodopsin variant D96N", *Opt. Lett.* **19** 1412 (1994).

[32] A. Kikineshy, Z. Bathory-Tarczy, I. Rosola, and J. Sharkany, "Materials and devices for fiber optic sensors", *Proceedings of NATO Advanced Workshop on Multichip Modules with Integrated Sensors, Budapest, Hungary, 18-20 May 1995*, pp. 181-4, eds. K.W. Jones and G. Harsanyi, Kluwer Academic Publishers, Dordrecht, Netherlands, 1996.

[33] A.S. Bablumian, T.F. Krile, D.J. Mehrl, J.F. Walkup, "Recording shift-selective volume holograms in bacteriorhodopsin", SPIE **3159**, 230 (1997).

[34] J.D. Downie, "Optical processing of speckle images with bacteriorhodopsin for pattern recognition", *Optics and Lasers in Engineering* **23**, 121 (1995).

[35] N. Hampp, and D. Zeisel, "Mutated Bacteriorhodopsins-versatile media in optical image processing", *IEEE Engineering in Medicine and Biology Magazine* **13**, 67 (1994).

[36] H. Rajbenbach, "Dynamic holography in optical pattern recognition", *SPIE* **2237**, 329 (1994).

[37] D. Oesterhelt, C. Bräuchle, and N. Hampp, "Bacteriorhodopsin: a biological material for information processing", *Q. Rev. BioPhys.* **24**, 425 (1991).

[38] C. Bräuchle, N. Hampp, and D. Oesterhelt, "Optical Applications of Bacteriorhodopsin and its Mutated Variants", *Adv. Mat.* **3**, 420 (1991).

[39] A.S. Bablumian, T.F. Krile, D.J. Mehrl, and J.F. Walkup, "M-type thick holograms in bacteriorhodopsin film with a high-divergence reference beam", *Appl. Opt.* **37**, 1350 (1998).

[40] C. Wang, M. Bacon, A.K. Kar, B. S. Wherrett, and R.L. Baxter, "Characterization of long M-state lifetime bacteriorhodopsin thin films for optical cache memory", *Japanese Journal of Applied Physics* **36**, 439 (1997).

[41] A. Hafiz, R. Magnusson, J.S. Bagby, D.R. Wilson, and T.D. Black, "Visualization of aerodynamic flowfields using photorefractive crystals", *Appl. Opt.* **28**, 1521 (1989).

[42] A. Popp, M. Wolperdinger, N. Hampp, C. Bräuchle, and D. Oesterhelt, "Photochemical conversion of the O-intermediate to 9-cis-retinal containing products in bacteriorhodopsin films." *Biophysical Journal*, **65**, 1449 (1993).

[43] F.H. Mok, "Angle-multiplexed storage of 5000 holograms in lithium niobate", *Opt. Lett.* **18**, 915 (1993).

[44] A.M. Darskii and V.B. Markov, "Shift selectivity of the hologram with a speckle reference wave." *Opt. Spectrosc.* **65**, 661 (1988).

[45] V.B. Markov, "Spatial-angular selectivity of 3-D speckle-wave holograms and information storage." *J. Imaging Sci. & Techn.* **41**, 70 (1997).

[46] L.O. Heflinger, R.F. Wuerker, and R.E. Brooks, J. *Appl. Phys.* Vol. 37, p. 642, 1966.

[47] J.E. O'Hare, "A Holographic Flow Visualization System," 14th Annual Technical Symposium Proceedings, Society of Photo-Optical Instrumentation Engineers, Volume 2, pp. 449-510, Sept. 1969.

[48] P. Hariharan, Optical Holography: Principles, Techniques and Applications, Cambridge University Press, Cambridge, 1984.

[49] R. Magnusson, X. Wang, A. Hafiz, T.D. Black, L. Tello, A Haji-Shekh, S. Konecni, and D.R. Wilson, "Experiments with photorefractive crystals for holographic interferometry," *Opt. Eng.*, Vol. 33, No. 2, pp. 596-607, February 1994.

[50] M.P. Georges, and P.C. Lemaire, "Phase-shifting real-time holographic interferometry that uses bismuth silicon oxide crystals," *Appl. Opt.*, Vol. 34, No. 32, 10 November 1995.

[51] J.E. Millerd, N.J. Brock, M.S. Brown and P.A. DeBarber, "Real-time resonant holography using bacteriorhodopsin thin films," *Opt. Lett.*, Vol. 20, No. 6, March 15, 1995.

[52] J.D. Trolinger, "Flow Visualization Holography," *Opt. Eng.*, Vol. 23, No. 5, pp. 470-481, 1975.

[53] T.A.W.M. Lanen, P.G. Bakker, P.J. Bryanston-Cross, "Digital holographic interferometry in high-speed flow research", *Exp. in Fluids*, Vol. 13, pp. 56-62, 1992.

[54] J.E. Grievenkamp and J.H. Bruning, "Phase Shifting Interferometry," Daniel Malacara, Ed., Wiley Interscience, *Optical Shop Testing*, p. 501, 1992.

[55] R. Smyth, R. Moore, "Instantaneous phase measuring interferometry," *Opt. Eng.* 23, pp. 361-364, 1984.

[56] C.K. Hong, H.S. Ryu, and H.C. Lim, "Least-squares fitting of the phase map obtained in phase-shifting electronic speckle pattern interferometry," *Opt. Lett.*, Vol. 20, No. 8, April 15, 1995.

[57] W. Merzkirch, Flow Visualization, Academic Press, 1987.